NASA-CR-204628

THE SOLAR-B MISSION

FINAL REPORT
of the
SCIENCE DEFINITION TEAM

Spiro Antiochos, Naval Research Laboratory, Chair
Loren Acton, Montana State University
Richard Canfield, Montana State University
Joseph Davila, Goddard Space Flight Center
John Davis, Marshall Space Flight Center
Kenneth Dere, Naval Research Laboratory
George Doschek, Naval Research Laboratory
Leon Golub, Harvard-Smithsonian Center for Astrophysics
John Harvey, National Solar Observatory, NOAO
David Hathaway, Marshall Space Flight Center
Hugh Hudson, Solar Physics Research Corporation
Ronald Moore, Marshall Space Flight Center
Bruce Lites, High Altitude Observatory, NCAR
David Rust, Applied Physics Laboratory, JHU
Keith Strong, Lockheed-Martin Solar & Astrophyics Laboratory
Alan Title, Lockheed-Martin Solar & Astrophyics Laboratory

June 9, 1997

Contents

1 INTRODUCTION

Solar variability is due to the energy that is generated deep in the Sun's interior by nuclear burning, carried to the surface by convective motions, and finally transported to the outer atmosphere and heliosphere by the Sun's magnetic field. This variable transport of energy is the origin of all the many manifestations of solar activity that drive the Sun-Earth connection. Magnetic fields play the central role in the variable transport of the Sun's energy. The solar magnetic field modulates the thermal energy that escapes the Sun's surface, the photosphere, in the form of black-body radiation, and the magnetic field carries directly the non-thermal energy that produces the dynamic corona and heliosphere. Variability in the Sun's nonthermal emissions drive space weather and variability in the thermal radiation is an important driver of global change.

Our view of solar variability has been revolutionized by Yohkoh, an ISAS mission with major NASA participation. Yohkoh has shown that the hot corona is extremely dynamic, with magnetic reconnection, rapid heating and mass acceleration being common phenomena. SOHO a joint ESA/NASA mission is now showing in detail the physical parameters of plasma heating and acceleration. The next vital step is to understand the magnetic origins of variability. Solar-B, the next ISAS mission, is designed to address this fundamental question of how magnetic fields interact with plasma to produce solar variability. Measuring the properties of the Sun's magnetic field is the fundamental observational goal of Solar-B.

The mission has a number of unique capabilities that will enable us to answer the outstanding questions on solar magnetism. First, by escaping atmospheric seeing, it will deliver continuous observations of the solar surface with unprecedented spatial resolution. Solar-B will allow us for the first time to observe the dynamics of the elemental, discrete magnetic flux tubes that form the photospheric magnetic field. It is the dynamics of these flux tubes that is thought to be responsible for the activity observed in the corona by Yohkoh.

Second, Solar-B will deliver the first accurate measurements of all three components of the photospheric magnetic field. In order to have the free energy necessary to power solar activity, the magnetic field must contain electric currents. It is vital, therefore, that all components of the field be observed so that the currents can be calculated. However, the magnetic components transverse to the line of sight are difficult to observe, and cannot be measured with any degree of accuracy if the field is not spatially resolved. By resolving the magnetic structures, Solar-B will yield measurements of the transverse field that will be truly revolutionary.

Finally, Solar-B will measure both the magnetic energy driving at the high-beta photosphere and, simultaneously, its effects in the low beta corona. The mission consists of a complement of instruments that will observe the solar surface and atmo-

sphere as one coupled system. This instrument complement contains an optical vector magnetograph for the photosphere and coordinated X-ray/XUV imaging telescopes and spectrographs for the corona. As in Yohkoh, the US would have full participation in all instruments and all the data. The US would contribute only one-quarter the cost of the mission; therefore, we would be able to obtain facility class science for a MIDEX price.

In addition to the many science rewards, Solar-B offers unique programmatic opportunities to NASA. It will allow us to continue our cooperation in space science with our most reliable international partner. Solar-B will deliver images and data that will have strong public outreach potential. The science of Solar-B is clearly related to the themes of origins and plasma astrophysics, and contributes directly to the national space weather and global change programs.

2 SCIENTIFIC OBJECTIVES

The overarching goal for the Solar-B mission is to comprehensively understand the solar photosphere and corona, as a system. To address this broad goal we identify four promising areas of exploration:

- Magnetic field generation and transport
- Magnetic modulation of the Sun's luminosity
- Heating and structuring of the chromosphere and corona
- Eruptive events and flares

Taken together, these topics encompass much of the effort by the US and international solar physics communities, and are at the heart of solar variability.

2.1 Magnetic Field Generation and Transport

Generation of magnetic flux is believed to take place through the interaction of solar rotation with the convecting, highly conductive plasma deep within the Sun. Once generated, magnetic flux rises through the convection zone to the visible solar surface. Recent results show that the topology of the magnetic fields, as they emerge into the visible atmosphere, reflects the workings of both the dynamo and the passage through the convection zone. The processes by which solar flux reconnects, erupts, and leaves the Sun to produce a solar cycle are unknown. Solar-B will observe the topological changes associated with magnetic flux emergence, reconnection, and eruption, through simultaneous X-ray and vector magnetic field observations.

Challenges of Solar Magnetism

Understanding the generation of magnetic fields, their emergence into the solar atmosphere, and their energetic consequences are challenging and fascinating problems in their own right. Not only does the study of the physics of the solar plasma have importance for understanding how the Sun influences the Earth and its space enviroment, it also provides a cornerstone for understanding magnetized plasmas occurring in other astronomical contexts.

Three aspects of solar magnetism have highest priority for Solar-B:

- The dynamo process within the Sun which is the origin of the solar magnetic cycle.
- The processes which govern the transport and subsurface evolution of magnetic fields as they rise to and penetrate the surface.
- The dispersal, decay, and ejection of magnetic energy and flux once the fields have emerged.

To address these challenges, the key strength of Solar-B is its capability to simultaneously observe coronal structure and photospheric vector magnetic field.

The Solar Dynamo

Magnetic fields of lower main-sequence stars such as the Sun are believed to arise from a dynamo process operating near the base of their convective envelopes. The magnetic field is generated through the interaction of solar rotation with the convecting, highly electrically conductive plasma. Evidence of this process is seen in the hemispheric dependence of the twist of active region magnetic fields (Figure 1), which recent studies have shown cannot simply be explained in terms of differential rotation or the dynamics of flux ropes rising through the convection zone. It is therefore believed that twisting of the magnetic field into flux ropes by subsurface flows is a principal physical action of the dynamo process. This twist of the magnetic field $\mathbf{B} = \nabla \times \mathbf{A}$, where $\mathbf{A}$ is the vector potential, contributes to the magnetic helicity $\mathcal{H} = \int \mathbf{A} \cdot \mathbf{B}\, dV$, a topological quantity of both theoretical and observational interest. This process is understood only in broad outline, as the best extant models of the solar and stellar dynamos lack the ability to predict fundamental observed properties of the solar magnetic cycle. New observational inputs are now possible, through vector magnetic field observations from space, which will enable advancement in this important area. A major goal of Solar-B is to strengthen our understanding of the solar dynamo.

To date we have only very limited knowledge of plasma motions and magnetic fields deep within the Sun where the dynamo is believed to operate, but our knowledge is rapidly improving as a result of recent developments in helioseismology: the

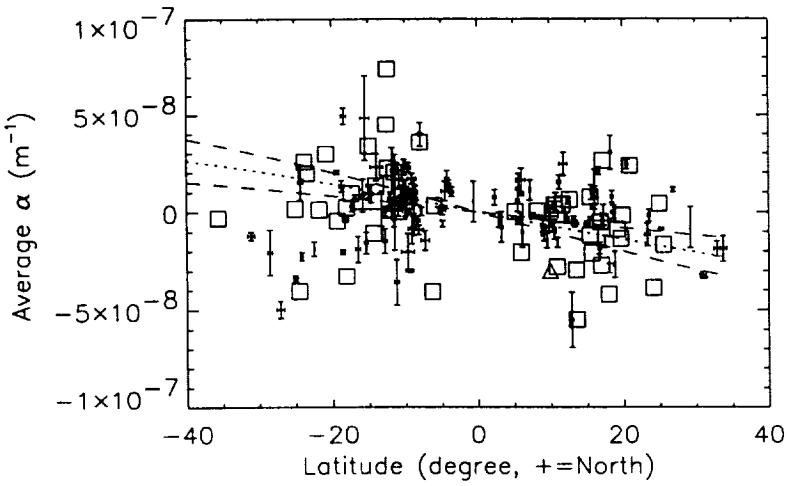

Figure 1: Observed latitude dependence of the large-scale twist (measured by the value of the force-free field parameter α of the magnetic fields of several hundred active regions observed from 1990 to 1996.

use of oscillations generated by the Sun itself to probe the physical conditions within, in an analogous fashion to methods developed by geophysicists to probe the Earth's interior. New observational programs of the coming decade, GONG for the ground-based effort and SOHO from space, will widen vastly our understanding of the solar interior. However, the magnetic fields measured at the surface, and their large-scale structure in the solar corona provide us with the most directly observable manifestation of the dynamo process. In particular, it is important to understand not only the spatial distribution of the polarity of magnetic fields at the solar surface, but also their geometric structure as they penetrate the solar surface and how they fill the coronal volume above. Thus, the combination of vector magnetic field structure at the solar surface observed simultaneously with the accompanying structure of the plasma in the solar corona (Solar-B), and the insight about subsurface flows derived from helioseismology (GONG and SOHO), will provide a unified observational picture of the dynamo process heretofore unattainable.

The ways in which Solar-B will most effectively contribute to this goal, through its novel combination of vector magnetic field measurements and X-ray images, are:

- Measurement of the global patterns of the topology of the emerging magnetic

field (handedness and density of twist),

- Measurement of the distribution of size scales for the twist of the magnetic field, an observable quantity fundamental to the dynamo process,
- Observational description of the modes of evolution and expulsion of magnetic flux and helicity from the Sun in relation to flux emergence, dispersal, and reconnection.
- Observational characterization of the role of reconnection and expansion of the flux into the corona on the fields below.
- Quantification, for the first time, of the flux history of individual solar active regions, through measurements of the vector magnetic field as an active region rotates across the solar disk.

Subsurface Transport and Flux Emergence

The evolution of magnetic flux as it is transported from its dynamo origin at the base of the convection zone, upward through the convecting and rotating solar envelope is surely geometrically complex. However, large-scale magnetic features such as prominences, active region complexes, and coronal holes (as well as overall active-region magnetic field twist, see Figure 1) suggest that the fields retain some of their twisted topology in spite of their journey through the turbulent envelope of the Sun (sinuous structures in Figure 2). Furthermore, recent theoretical work has indicated that it may not be possible for the Sun to transfer large-scale helicity to smaller and smaller scales, so that the solar magnetic field retains its large-scale helicity even after it penetrates the surface.

SOHO observations of the emergence of magnetic fields at the smallest scales yet observed show that the process is a complex one. As well, it is a continuous one, in which new flux emerges in the form of very small bipoles (ephemeral regions). Each bipole, on average, bring to the surface a total flux of about 10^{19} Mx. These bipoles bring enough flux to the surface to replace all of the magnetic field on the Sun on a time scale of 20 to 100 hours. The total field in the quiet Sun is 10 to 100 times more than the net flux. The observed distribution of flux concentrations, the number of a given flux versus flux at the SOHO resolution, can be predicted on the basis of a statistical mechanical model based on the assumptions that fields moving along intergranular boundaries have a given probability of merging and canceling, and that they spontaneously fragment in proportion to the amount of flux in the concentration. The merging, cancellation, and fragmentation rates have been measured and it has been possible to predict the flux distributions of both polarities in very quiet Sun and dense plage. When the flux concentrations observered at SOHO resolution are

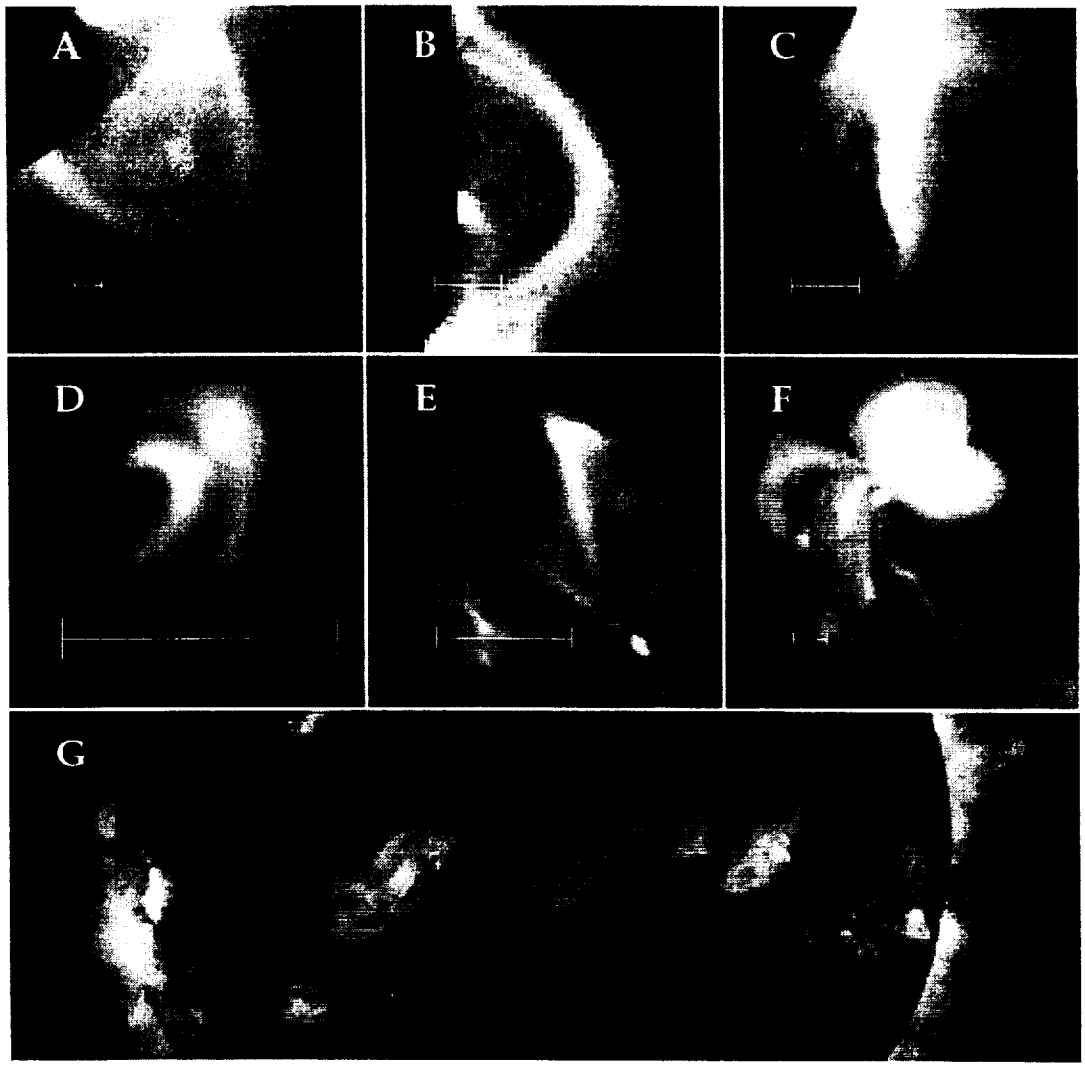

Figure 2: Examples of the structuring of the X-ray corona by the magnetic field, illustrated by selected images from Yohkoh. A) helmet type streamer; B) arcade of loops seen end-on; C) dynamic eruptive ejection with twist; D) flaring loops, loop-top heating; E) wishbone-shaped loops with cusps, one with heating concentration in the cusp; F) loops; and G) S-shaped structures between active regions. (Courtesy Lockheed Martin Solar & Astrophysics Group.)

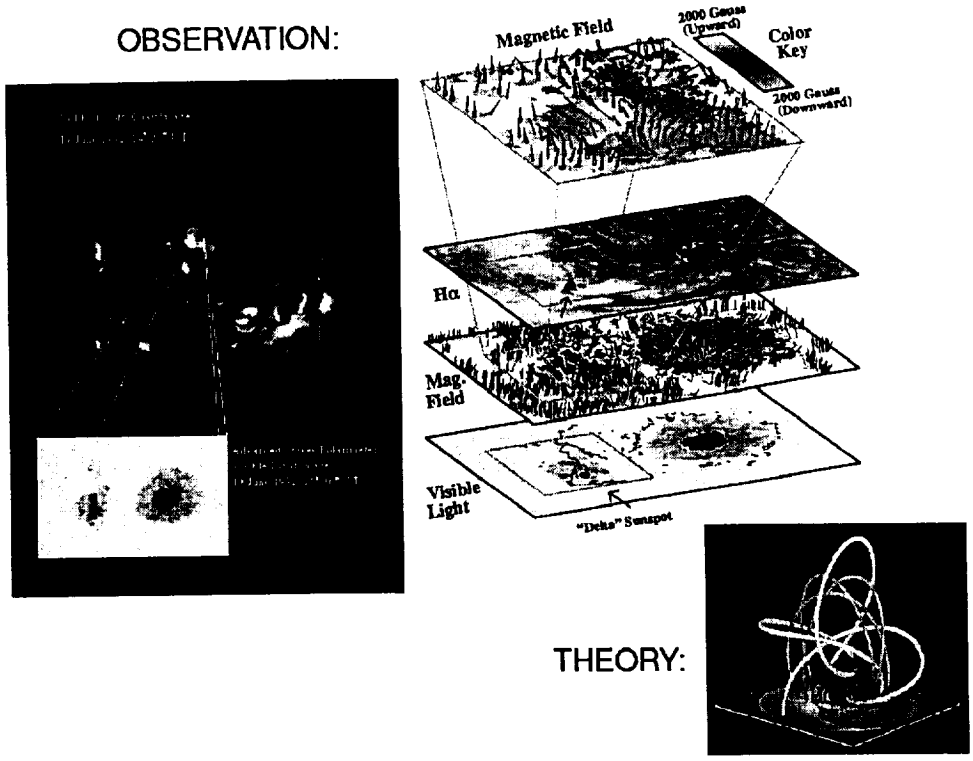

Figure 3: Theoretical toroidal flux-rope model of the magnetic field of a "Delta" spot, based on observations from the ground-based Advanced Stokes Polarimeter (center) and Yohkoh (left). The ASP vector magnetic field maps show the *concave upward* nature of the vector field present in the small "delta" sunspot at the left. The corresponding narrow-band chromospheric image in $H\alpha$ shows the presence of a prominence "filament" forming directly above the line separating fields of opposite magnetic polarity. The theoretical model of the 3-dimensional magnetic field geometry appearing at the lower right shares many features common to both the vector fields observed at the photosphere and the twisted nature of the field lines in the corona as inferred from the X-ray images. Some field lines in the theoretical model appear to bridge the opposite polarities along straightforward paths. Others take more circuitous paths which experience one or more local minima *above the photosphere*. The minima of some such field lines are shown, suggestive of cool prominence material residing stably in the corona, isolated from the high temperature corona by the magnetic field.

examined at higher resolution with groundbased magnetograms, the concentrations are observed to break up into smaller fragments that are embedded in the intergranular lane pattern just as the concentrations at the MDI resolution are embedded in the supergranular pattern.

A new generation of instrument capable of providing vector magnetic field measurements is needed to quantitatively describe the state of the magnetic field as it emerges. The magnetic field is a vector quantity, and it is not sufficient to measure only one component of this vector to answer the questions we pose. This information is crucial not only to understanding the large-scale evolution of the field which concern the dynamo process, but also the topology of structures of the outer atmosphere of the Sun, as shown dramatically in Figure 3. Several important questions regarding subsurface flux transport and emergence may be addressed by Solar-B:

- Does the natural buoyancy of magnetized plasmas drive the emergence of magnetic flux, or are the inductive effects of flows such as differential solar rotation, meridional, supergranular, and granular flows important, as well?
- What is the magnetic flux history of individual solar active regions, during the process of flux emergence? Does flux submergence play a significant role?
- Does submergence of magnetic fields commonly occur, presumably as a result of magnetic tension forces in curved subsurface magnetic fields, or is this phenomenon rare due to both buoyancy and the rapid expansion of field structures into the corona?

Dispersal, Decay, and Ejection of Magnetic Fields

The processes by which the magnetic flux of solar active regions disappears from the solar surface remain largely unknown, yet we know such processes must exist because the net polarity of the magnetic field in each hemisphere reverses with each 22-year magnetic cycle. It is suspected that sunspot magnetic fields are dispersed, through the action of turbulent convection, into the quiet Sun in the form of many very small, intense magnetic flux tubes, which comprise the magnetic network of the quiet Sun. Their fate from that point on is even more speculative, but either they undergo reconnection and dissipation in the form of micro-flares and atmospheric heating, or they are ejected into the corona and solar wind. As yet, these speculations have been neither refuted nor supported because we lack the high resolution, continuous observations of the photospheric magnetic field which Solar-B will provide.

In order for the solar magnetic polarity to reverse itself every 11 years, it is probably necessary for the Sun to expel the large-scale twisted field structures, in the form of coronal mass ejections. There is no other obvious avenue for the Sun to dissipate the large-scale helicity which clearly appears to be present in solar magnetic fields in

the form of the long chromospheric filaments which commonly reside at high latitudes. Interestingly, the extremely high resolution magnetic observations from Solar-B are absolutely necessary to define the nature of even the largest scale structures of the solar magnetic field and its resulting coronal structure.

The most important objectives of Solar-B magnetic field measurements for elucidating the processes by which magnetic flux evolves are:

- To identify the modes of decay and dispersal of active regions in quantitative terms, allowing for the contributions to the flux loss by reconnection, ejection, and dissipation into the quiet magnetic network,
- To explore the physical properties of the intense, but very small magnetic flux tubes which apparently are responsible for most of the 11-year periodic variability of the net radiative output of the Sun,
- To determine the fate of quiet region magnetic flux by in-situ dissipation of the accompanying electric currents (leading to atmospheric heating, either impulsive or steady), by reconnection (leading to small scale ejection of magnetic flux – a process not yet observed but within the capability of Solar-B instruments), or even by submergence, and
- To determine the nature and importance of turbulent, weak internetwork magnetic fields in the context of the apparently dominant intense fields.

Whenever quantitative magnetic flux measurements are called for, as in the objectives stated above, measurement precision is essential. Solar-B will provide the first opportunity to explore vector magnetic fields with sufficient precision and temporal continuity to address these fundamental objectives.

2.2 Magnetic Modulation of the Sun's Luminosity

The Sun is known to vary on many time scales. On short time scales, it varies in its total luminosity due to both the global p-modes and due to granular convection in a nearly random fashion with characteristic times of a few minutes, and with an amplitude of a few times 10^{-5}. The quasi-periodic solar luminosity variability at longer periods is roughly a hundred times greater in amplitude. Time scales for these components of the solar luminosity spectrum range from the shortest observable times associated with solar flares and other dynamical events, through the daily and monthly evolutionary times of active regions, to the decadal time scales of the solar cycle, and even to time scales of centuries associated with long-term variations of solar activity. The underlying cause of this dominant component of solar variability

is the Sun's magnetic field. Variable solar magnetic activity is therefore the dominant source of all those fluctuations in the solar output deemed important to the Earth and its space environment.

Understanding the magnetic origin of this variability – the generation of the magnetic fields, their emergence into the solar atmosphere, and their energetic consequences – is a challenging and fascinating problem, discussed above. Ultimately, the prediction of solar variability at all wavelengths will most likely hinge on a firm physical understanding of the solar processes involved. Solar-B is a mission which is poised to make unprecedented advances in our understanding of solar magnetism as a global process, and specific advances toward understanding the magnitude and cause of solar luminosity and spectral irradiance variations, as outlined below.

Accounting for Sources of Solar Luminosity Variations

That the solar luminosity varies with the 11-year solar activity cycle at the level of 0.1 - 0.2% has been clearly demonstrated by several space-borne experiments during the last 17 years. Short-term dips in the luminosity at times of high activity are due to the presence of sunspots. For some time the source of the long-term luminosity variations was believed to be solar *faculae*: intense, small scale magnetic elements outside of sunspots which appear brighter than the unmagnetized quiet Sun when viewed away from disk center, shown in Figure 4.

Recently, however, attempts to account for the luminosity changes due to observed measures of facular brightening have come up short: there appears to be a component of the luminosity variation which remains unaccounted for in budgets of solar luminosity variations. A central issue is therefore to identify the source and the physical mechanisms responsible for all of the observed solar luminosity variations. Solar-B can contribute in a unique way to this understanding.

Ground-based efforts are now underway to attempt to identify the global (i.e., full-Sun) irradiance variations with specific solar features (the NSF SunRISE program). Such identifications are however limited by one's ability to identify the structures through the blurring effect of the Earth's atmosphere. With the broad-band imaging of the solar photosphere with Solar-B, one may account for all the intensity variations of the solar surface within an active region-sized portion of the solar disk. Thus the local sources of brightness variations may be recorded, and catalogued using images of unwavering high quality, thus removing the ambiguity inherent to any ground-based measurement. The unwavering superb angular resolution of the Solar-B imaging magnetograph, along with its extremely high sensitivity to magnetic fields, will permit for the first time an accurate assessment of the luminosity variations attributable to magnetic fields *outside of active regions.* Magnetic fields in the quiet Sun may be the source of the unidentified component of luminosity variation, especially considering that recent ground-based and SOHO measurements have identified the importance of

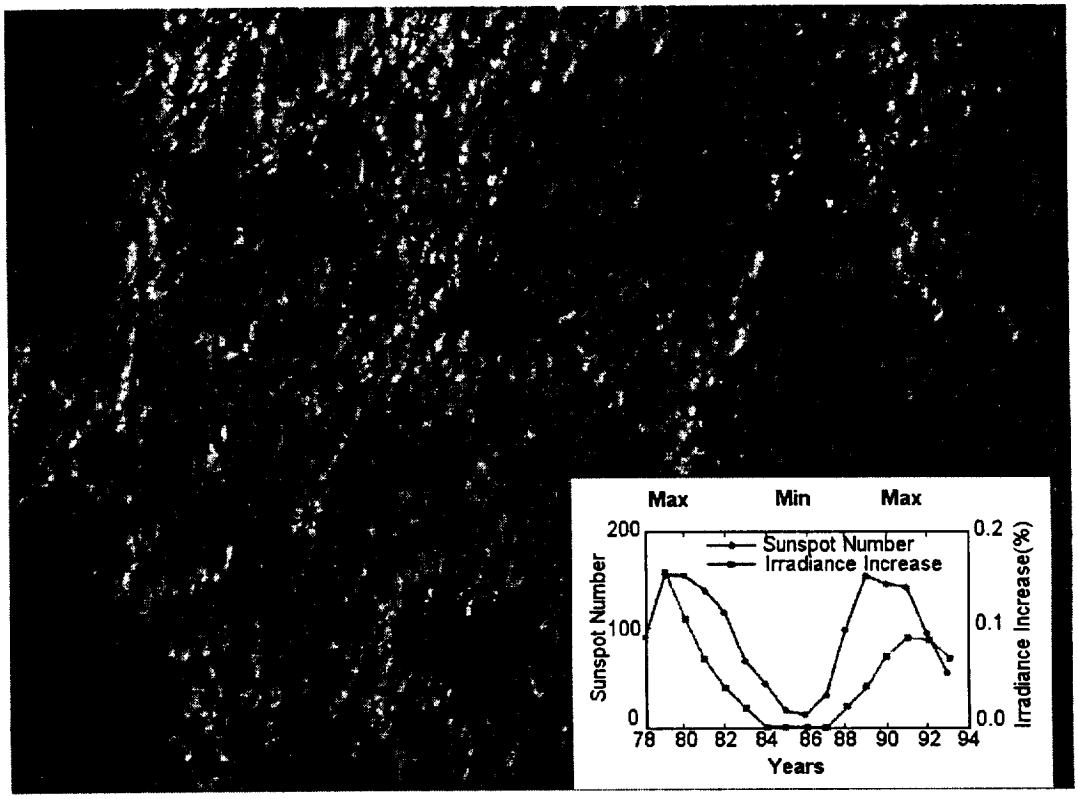

Figure 4: Visible continuum image of the bright faculae in and around a sunspot group. The supergranular cell/network pattern is seen in the outskirts of this region. The spatial resolution is about a quarter of an arcsecond, enough to show the photospheric granulation quite well. Each bright facular element marks a magnetic flux fragment. The magnetic and flow fields in each fragment somehow result in the enhanced photospheric emission, which when summed over all faculae accounts for much of the rise and fall of the the solar luminosity with the sunspot cycle. Because of blurring by turbulence in the Earth's atmosphere, even at the best sites ground-based observatories obtain only rare glimpses of the Sun at this resolution (0.25 arcsecond). Because of the perfect seeing in space, the 50 cm telescope on Solar-B will provide continuous viewing of the photosphere and chromosphere at this resolution. (G-band image from the 50 cm Swedish Vacuum Telescope on La Palma.)

the non-active region fields. With Solar-B, detailed studies of the root causes of solar luminosity variations may be carried out during the rapidly changing declining phase of the solar activity cycle. It may be possible to determine trends in the relative contributions of active region and quiet region magnetic fields to the observed global luminosity variations.

Solar-B will provide the first capability for precision diagnostics of the evolution of solar magnetic features at high angular resolution. This will enable one to investigate in detail the underlying radiative and magnetohydrodyamic processes governing these structures, and thus enable us to understand the physical basis for the solar luminosity variations. With Solar-B's breakthrough to steadfast subgranular spatial resolution, we will be able to answer the following questions:

- How do the brightness and lifetime of a facular element depend on the strength, total flux, and inclination of the magnetic field in the element?
- How is the magnetic field that forms a facular element assembled by the granular flow and how is it dispersed in the demise of the facular element?
- Are facular elements predominantly unipolar, or do they occur preferentially between colliding magnetic field clumps of opposite polarity?

Spectral Irradiance Variations

The solar radiative output is increasingly more variable as the wavelength of the emitted radiation decreases. Such variations have a major influence on the Earth's upper atmosphere, and as a result, may also influence climate variations. Just as with the luminosity variations, nearly all of the irradiance variations at short wavelength may be traced directly to the injection of magnetic fields into the solar atmosphere. Besides being an important driver of the space environment of the Earth, the magnetic heating and dynamics of the outer solar atmosphere presents us with the best opportunity to understand the physics of related processes common to a wide range of other astrophysical systems. The power of Solar-B to address these fundamental questions surrounding the heating and structuring of the outer solar atmosphere is the topic of the following section.

2.3 Structure and Heating of the Chromosphere and Corona

The forces that dominate in the dense photosphere differ substantially from those which dominate in the upper layers of the solar atmosphere. For the most part, hydrodynamic forces dominate in the photosphere, and only within the strongest magnetic field structures, such as sunspot umbrae, do magnetic forces rival the hydrodynamic forces. However, the density of the solar plasma falls off very rapidly

with height due to the extremely small scale height low in the solar atmosphere, so that in the higher layers of the atmosphere the magnetic field often dominates its dynamics and structure. The structure imparted by the magnetic field gives rise to the phenomena we observe in these structures, and it also strongly affects physical processes leading to heating of the atmosphere. Thus, understanding the nature of the various phenomenological structures we observe in the solar atmosphere will provide important links toward understanding the nature of the heating of the outer atmospheres of stars.

Chromosphere

In the chromosphere a complex arrangement of magnetically-dominated and relatively field-free regions is observed. It appears that in non-magnetic chromospheric regions, acoustic heating is likely to be the dominant energization process. Photospheric convective motions generate sound waves which may steepen into shock waves that dissipate to heat the field free regions of the chromosphere, such as in the centers of supergranule cells. The emission from magnetic regions of the chromosphere is well known to be in excess of that in non-magnetic regions; hence, some additional heating must occur due to the presence of the magnetic field. The enhanced chromospheric heating in the magnetic network could be due to the turbulent motions of the upper convection zone which generate MHD waves that travel outward in the flux tubes. Dissipation of this wave energy could give rise to the enhanced chromospheric emission seen in the magnetic lanes of the network.

Solar-B will enable us to follow the shocks and their heating with height in the chromosphere and transition region by observing appropriate EUV lines through imaging spectroscopy (see Figures 5 & 6) with high spatial, temporal and spectral resolution. With its vector magnetograms of high spatial resolution, Solar-B will easily be able to distinguish the magnetic field at the boundaries of the supergranular cells from their relatively non-magnetic interiors. Simultaneous observations of the magnetic field and of longitudinal and transverse motions will help us gauge the nature and magnitude of the generation, propagation and dissipation of these waves that could provide most of the heating of the hottest part of the solar chromosphere. Interesting questions which we can address with this unique combination of Solar-B observing capabilities include:

- Are non-magnetic regions of the chromosphere heated by shocks?
- How are magnetic regions of the chromosphere heated, and why are they so different from the field free regions?
- How is convective energy transferred from the photosphere to the corona?

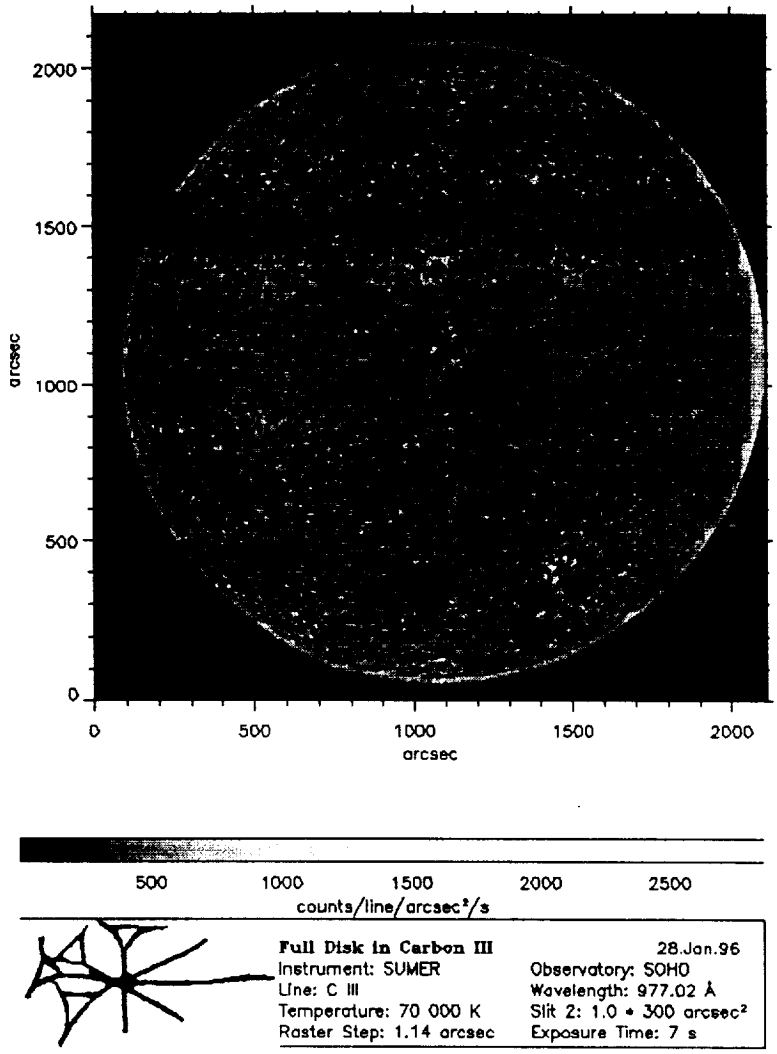

Figure 5: A full disk image showing the structure of the chromosphere in CIII built up from a series of slit spectrograph images. (Image provided courtesy of the SOHO/SUMER instrument team. SOHO is a cooperative mission between ESA and NASA).

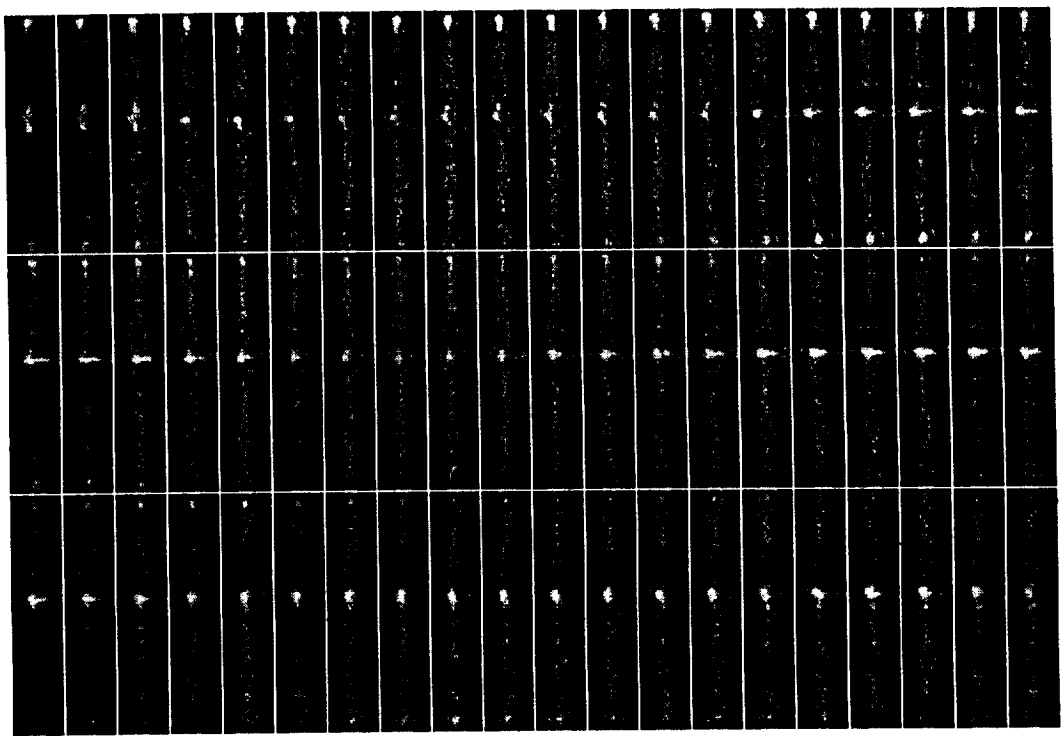

Figure 6: Explosive events observed by SUMER on 28 March 1996 in the emission line of Si IV at 1393 A, formed in the transition region at about 100,000 K. The picture shows a time series of 60 Si IV spectra, each with an exposure time of 10 s, covering a time interval of 10 minutes altogether. The spectral window is 25 pixels, allowing observations of redshifts (to the left) and blueshifts (to the right) up to approx. 100 km/s. The north-south extension of the slit covers approx. 84.000 km on the Sun (120 arcsec). (Image provided courtesy of the SOHO/SUMER instrument team. SOHO is a cooperative mission between ESA and NASA).

Corona

It is well known from Yohkoh and EIT images that coronal emission is highly structured (see Figure 7). A number of recent studies have emphasized the importance of thermally differentiated imaging as part of the program to understand the heating and structuring of the solar corona. It has long been known that very different structures are seen in ground-based eclipse data in, e.g., the 'red line' (Fe X) compared with the 'green line' (Fe XIV). In soft X-ray observations, this point has been summarized by noting that the observed coronal loop structures may be viewed as relatively isolated mini-atmospheres, each with its own temperature and density structure. Because of the marked difference in observed coronal parameters within small spatial distances, it appears that the coronal heating mechanism can have markedly different effectiveness in portions of the atmosphere which are otherwise indistinguishable. This idea was made evident by observations such as the simultaneous NIXT and Yohkoh SXT comparison which were carried out in April 1993.

Although the overall appearance of an active region observed in the two pass bands is the same, close examination indicates that substantially different structures are seen at 2.5 x 10^6 K in the NIXT vs. 4 x 10^6 K in the SXT. The comparison shows that there are clusters of loops seen in one temperature range which are entirely invisible in the other: this effect works in both directions, so that both instruments fail to detect structures which are present in the corona and which must be presumed to play a role in coronal dynamics. The conclusion from this work is that instrumentation which detects an entire series of successive ionization stages of the same element is needed, in order to not "miss" any of the emitting material.

It is generally agreed that the heating of the corona and chromosphere is driven by convective motions in the photosphere, and that the transfer of energy is somehow mediated by the magnetic field.

Two broad classes of theories have been developed to explain how the kinetic energy of convection is thermalized in the corona. (1) Rapidly fluctuating motions may produce MHD waves which propagate into the corona where they are resonantly absorbed. The wave theory is able to reproduce the coronal structuring and the necessary heating rate, however unambiguous evidence for sufficient wave power in the corona has never been obtained. (2) The second broad class of heating mechanism suggests that the corona may be heated by the dissipation of electric currents. These currents are generated by the slow, shuffling motions of the magnetic flux bundles in the photosphere, and the subsequent twisting and braiding of the coronal magnetic field. In the corona these currents are resistively dissipated in thin current sheets.

As new magnetic flux erupts from below the photosphere, previously emerged flux must be dissipated or ejected into the solar wind to maintain a steady state. Reconnection is a process by which the free energy contained in non-potential magnetic fields (or, equivalently, contained in the electric currents which support them) may

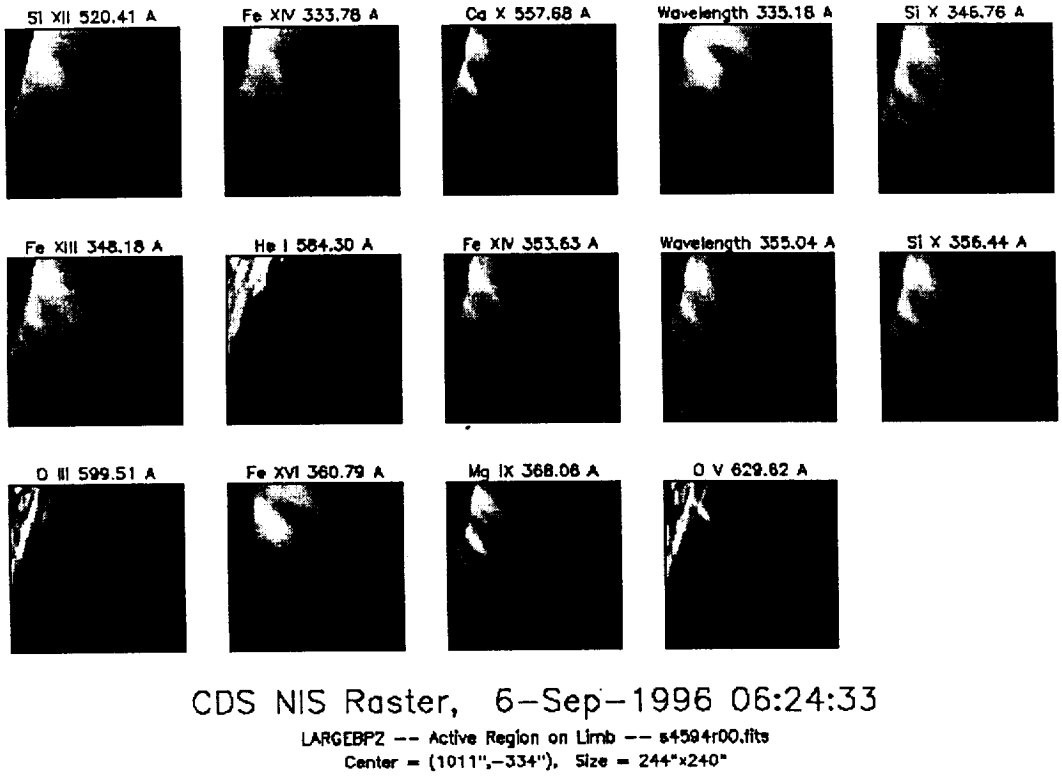

Figure 7: Images of a set of coronal loops as seen at the solar limb in emission lines representing temperatures from 100,000 K to about 4 x 10^6 K. Images were constructed by rastering the slit. These images demonstrate the strong temperature gradients present in the corona. (Image provided courtesy of the SOHO/SUMER instrument team. SOHO is a cooperative mission between ESA and NASA).

SOHO views of polar plumes
1996 March 7

Top to bottom:
MDI hi-res magnetogram
EIT Fe IX/X 171 Å image
EIT He II 304 Å image

Figure 8: These images by the Extreme-ultraviolet Imaging Telescope (EIT) on board SOHO show ultraviolet images of polar plumes near the south solar pole at about 1.5 million degrees Celsius in the Fe XII emission line at 195 A (top) and at somewhat cooler temperature at about 1 million degrees in the Fe IX/X emission lines at 171 A (bottom). These images represent the first opportunity scientists have had to see the detailed development over time of the plume structures, at least at the solar poles. (Image provided courtesy of the SOHO/MDI and EIT experiment teams. SOHO is a cooperative mission of ESA and NASA).

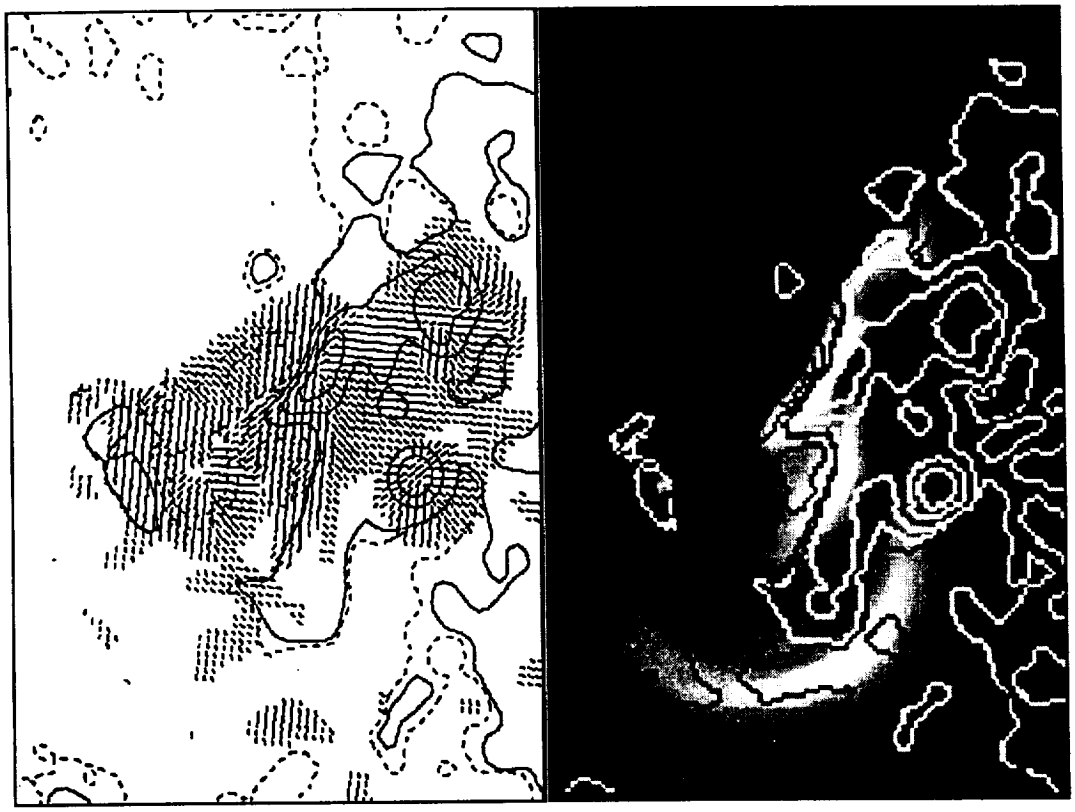

Figure 9: Comparison of the X-ray corona of an active region with the roots of its magnetic field in photosphere. The X-ray emission is brightest where coronal heating is strongest, showing that in this active region the strongest heating was in the most strongly stressed (most nonpotential) magnetic field. The left panel shows a vector magnetogram of AR 6982 (from the NASA/MSFC solar observatory); the strength of the line-of-sight component of the magnetic field is shown by the contours (solid for positive polarity, dashed for negative polarity), the direction and strength of the transverse component of the field are shown by the direction and length of the distributed tic marks. The right panel shows a coronal X-ray image of this active region (observed by Yohkoh) superposed on the line-of-sight field contours (white for positive; black for negative).

be transformed rapidly into heating, mass motions, and/or structural changes of plasmas, and it likely plays the dominant role in the continual readjustment of the global solar field. The Yohkoh mission represents a milestone in the observation of coronal magnetic structures, and has demonstrated the large variety of magnetic topologies which can exist in the corona (Figure 2). It has provided particularly strong evidence for magnetic reconnection on a wide range of size scales. Solar-B, with its unique combination of crucial magnetic field measurements in the photosphere and high resolution observations of the solar corona, will be ideally poised to address the following important questions regarding the role of heating and reconnection in the magnetic evolution of the solar atmosphere:

- What processes lead to the open magnetic field structures which dominate the mass flux of the solar wind, yet which apparently extend down to the base of the corona?
- How does the magnetic field support and thermally insulate the cool condensations, such as prominences, embedded in the solar corona?
- What are the relative roles of in-situ coronal reconnection and evolution of the photospheric magnetic field for structuring of large-scale coronal magnetic structures?

The bulk of the hot coronal plasma is in the form of loops. Each loop is believed to correspond to a magnetic flux tube. Motions at the foot points of magnetic loops are believed to give rise to the heating which results in the X-ray emission of the loop plasma. There are two major classes of proposed heating mechanism: (1) slow motions shear the magnetic field and generate electrical currents which can heat the atmosphere by ohmic dissipation, or result in localized impulsive heating by reconnection (e.g. microflares) and (2) rapid shaking of the flux tubes generates MHD waves which when dissipated also could heat the coronal plasma. Both must be present to some degree; however, which of these mechanisms is dominant? Figure 9 illustrates the puzzle posed by observations having moderate spatial resolution. The transverse field is highly sheared along part of the polarity inversion line. The right panel shows a Yohkoh SXT image of the region, with selected longitudinal field strength contours superposed. Although much of the enhanced heating is in obviously highly stressed fields, some is not.

Another possibility for the heating of the magnetic regions of the chromosphere is microflaring seated in the mid to low chromosphere. This would require a mixture of opposite polarities on arcsecond to subarcsecond scales in the heated areas. The microflaring might be the source of spicules and waves that in turn contribute to the heating of the chromosphere and corona. A high-resolution vector magnetograph

in space (such as envisioned for Solar-B) will reveal whether or not the requisite mixture of polarities is present, and whether the mixed-polarity fields contain enough free energy (e.g. shear).

- Is the heating dominated by the dissipation of waves or electric currents?
- Is the heating mechanism different for active regions, the quiet Sun, and coronal holes?
- What is the role of spicules and macrospicules in the transport of mass and energy between the chromosphere and corona?

2.4 Eruptive Events and Flares

Some of the most fundamentally important effects that force changes in our local space environment originate in eruptive events on the Sun. Solar eruptions range over orders of magnitude in size, duration and energy output. Examples of such events vary in size from spectacular flares and coronal mass ejections (CMEs), which have direct and measurable effects on the Earth, to innumerable tiny spicules and coronal jets, which may only impact the Earth indirectly – through their coronal heating and subsequent solar wind generation. This leads us to the basic question:

- Are these highly diverse eruptive phenomena caused by the same fundamental physical processes? If so, what are they?

Eruptive events can be very rapid. This requires, for the larger events at least, that the energy be stored in the corona and released in a catastrophic manner. Hence, we must understand:

- How is a critically unstable state produced by energy buildup?
- How is the eruption triggered?
- How does the eruption propagate?

To accomplish these ambitious goals we have to be able to probe the solar photosphere with high spatial resolution to determine the evolution of the vector magnetic field, which is an indicator of free energy buildup. In addition we need to determine the topology, location and timing of the energy release. The determination of these boundary conditions will require high-resolution and high-cadence coronal imaging. To understand the physical and dynamic environment of the energy release process to help constrain MHD models, we will also need coronal spectroscopy with high

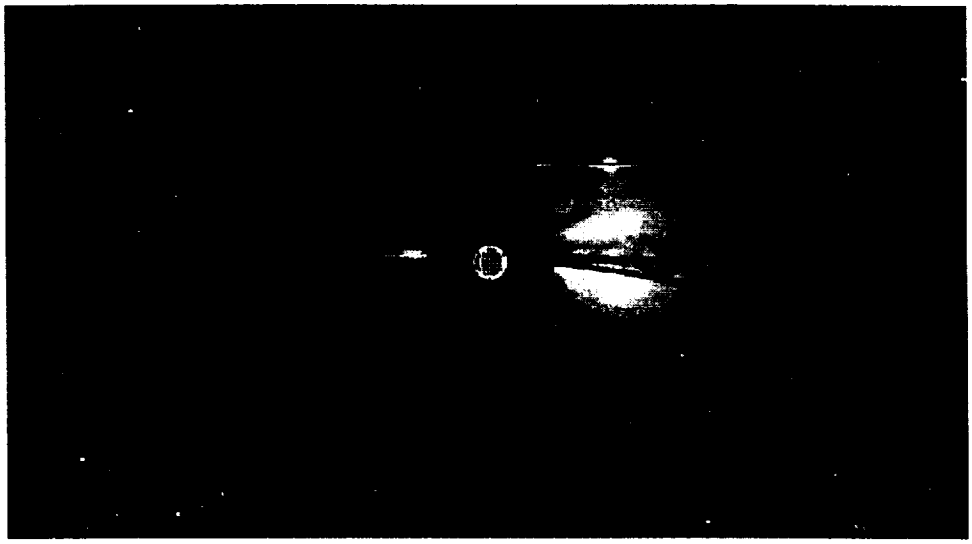

Figure 10: Large coronal mass ejection (CME) observed by the LASCO C3 coronagraph on SOHO. The size and location of the Sun are shown by the white circle in the center of the shadow of the occulting disk.

spectral resolution. Solar-B will supply the broad new observational view needed for this purpose.

The recent results from SOHO EIT show clearly that even at solar minimum the Sun is almost continuously producing eruptive events over a wide range of spatial and temporal scales. Solar-B will be launched during the declining phase of the current cycle and therefore should see a full range of solar activity levels from intense flaring to quiet solar-minimum conditions. Consequently, Solar-B will be an ideal tool to investigate the evolution of the magnetic field that leads to plasma erupting from the Sun.

The Buildup to an Eruption

Eruptions can happen rapidly (in seconds) so there is insufficient time to transport energy from remote sources and have a mechanism capable of dissipating it efficiently and quickly enough. Hence it is generally accepted that the energy is stored in nonpotential (sheared) coronal fields prior to the event. But the question remains as to how the fields become sheared. Possible explanations for the origin of these magnetic stresses include:

- Footpoint motion caused by the convection flows visible in the photosphere;

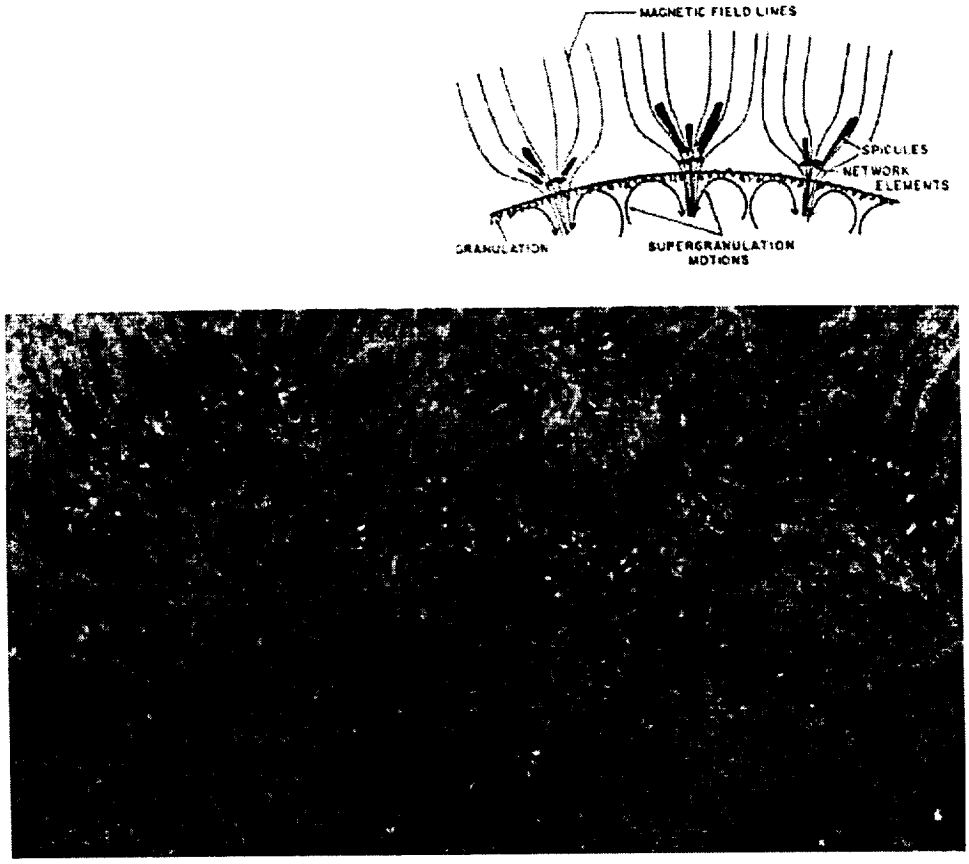

Figure 11: Spicules. Top: side-view sketch of the clustering of spicules in the magnetic network formed by supergranule convection cells. Bottom: high-resolution H-alpha filtergram from Hida Observatory.

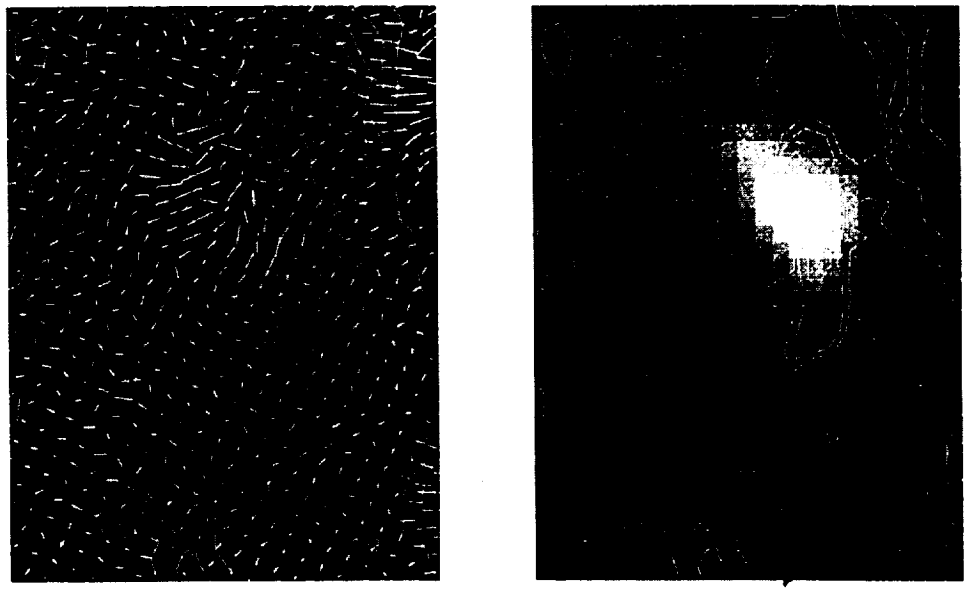

Figure 12: Characteristic magnetic shear at the site of an eruptive flare. The right panel shows a Yohkoh soft X-ray image of an eruptive flare during its explosive phase (the diffuse feature to the lower left is being formed by ejection of hot plasma from the bright core region); the X-ray image is superposed on contours of the line-of-sight component of the photospheric magnetic field (solid contours for positive polarity, dashed contours for negative polarity); the bright core of the flare straddles a polarity inversion line in a region on strong ($\sim$ 1000 gauss) magnetic field. The left panel shows a Mees Solar Observatory vector magnetogram with the same field of view as the right panel; the bold dashes show the strength and direction of the transverse component of the photospheric magnetic field (the strongest transverse field along the inversion line under the flare is $\sim$ 1000 gauss); the line-of-sight field component is shown by the same contours as in the upper panel (contour levels: 100, 200, 400, and 800 gauss). The field along the inversion line is seen to be strongly sheared, relative to what one would expect of a potential field.

- Proper motions of flux tubes in the photosphere due to the rotation or relative motion of sunspots;
- The emergence of magnetic field stressed far below the photosphere, perhaps by the solar dynamo itself.

The answer, of course, could be a combination of these physically different mechanisms.

Solar-B will be able to follow the build up of energy in the magnetic field because of its unique vector magnetogram capability and its orbit. Such measurements are not possible from the ground, at the high spatial resolution available to Solar-B, because of the image distortion due to the Earth's atmosphere. Equally importantly, Solar-B will have continuous coverage of the Sun because it is in a Sun-synchronous orbit. In contrast ground based observatories can observe only 6-8 hours each day assuming the best of conditions. The Solar-B view of the changing magnetic fields will produce a revolution in our understanding of the emergence and dissipation of the strong solar magnetic fields.

A question that has troubled solar observers for years concerns the existence of coronal signatures prior to an eruption. Solar-B with its high cadence, continuous coverage and the high spatial resolution of its coronal images and spectra should be able to identify any coronal indicator of the build up of energy, e.g., an increasing shear of the coronal loops with respect to the neutral line, changing energy dissipation in the loops or increased dynamic activity (turbulence or flows). The identification of such a signature could, for the first time, allow us to make reliable predictions of solar eruptions, one of the primary goals of the space weather program.

Triggering Solar Eruptions

There are several possible mechanisms to explain the triggering of an eruptive flare or coronal mass ejection. It can be driven by an essentially ideal process such as a kink instability or a resistive instability (e.g., tearing). Yohkoh has already demonstrated the importance of reconnection in the flare process by showing the dramatic evolution of the coronal fields as the result of such events. While this can be accounted for by the relaxation of the field after the event (i.e., after the explosive eruption of the magnetic field) there is still the intriguing idea that reconnecting magnetic field may also be the origin of the instability.

Solar-B can attack the problem of the triggering mechanism in a number of ways using combinations of the vector magnetic field and coronal imaging data. For example, the new observations can:

- Locate the time and the site of the initiation of the energy release

Figure 13: Large eruptive flare on the limb; soft X-ray image from Yohkoh. This spiked-top flare arcade is typical of flares that develop in tandem with a coronal mass ejection and are centered in the stressed magnetic field that explodes to drive the ejection.

- Determine the critical state of the coronal and photospheric fields at the time that the magnetic configuration becomes unstable and erupts
- Determine at what stage of the event the coronal fields reconfigure
- Derive changes in the 3-D field configuration, including topology changes, throughout the event
- Determine physical parameters in the eruptive and pre-eruptive plasma such as temperature and turbulence

Transport Effects

The combination of Yohkoh and SOHO is proving to be a very powerful tool in understanding the propagation of solar eruptions, particularly CMEs. However, Solar- B will determine the vector magnetic field during these phenomena. It will also bring much superior (continuous) coverage, plus higher spatial and temporal resolution. Solar-B will definitively follow the changes in the magnetic configuration of a region during an eruption. There is also the tantalizing prospect of seeing a relaxation directly in the photospheric fields and consequently being able to derive a self-consistent energy budget for such an event.

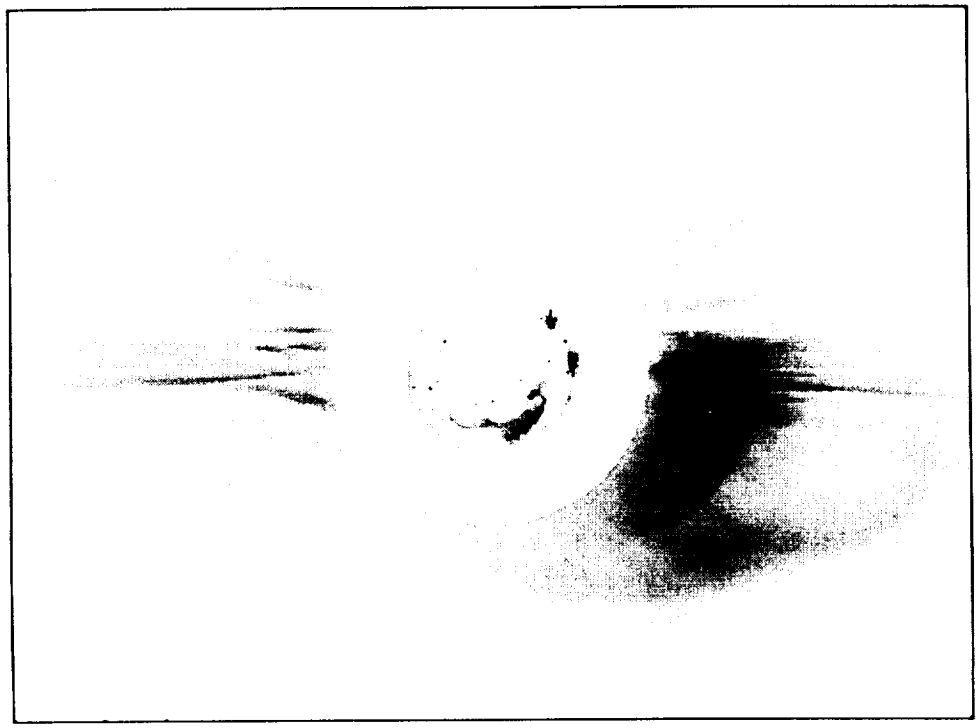

Figure 14: Large coronal mass ejection observed by the SOHO LASCO C2 coronagraph, and superposed simultaneous flare arcade observed by the Yohkoh SXT.

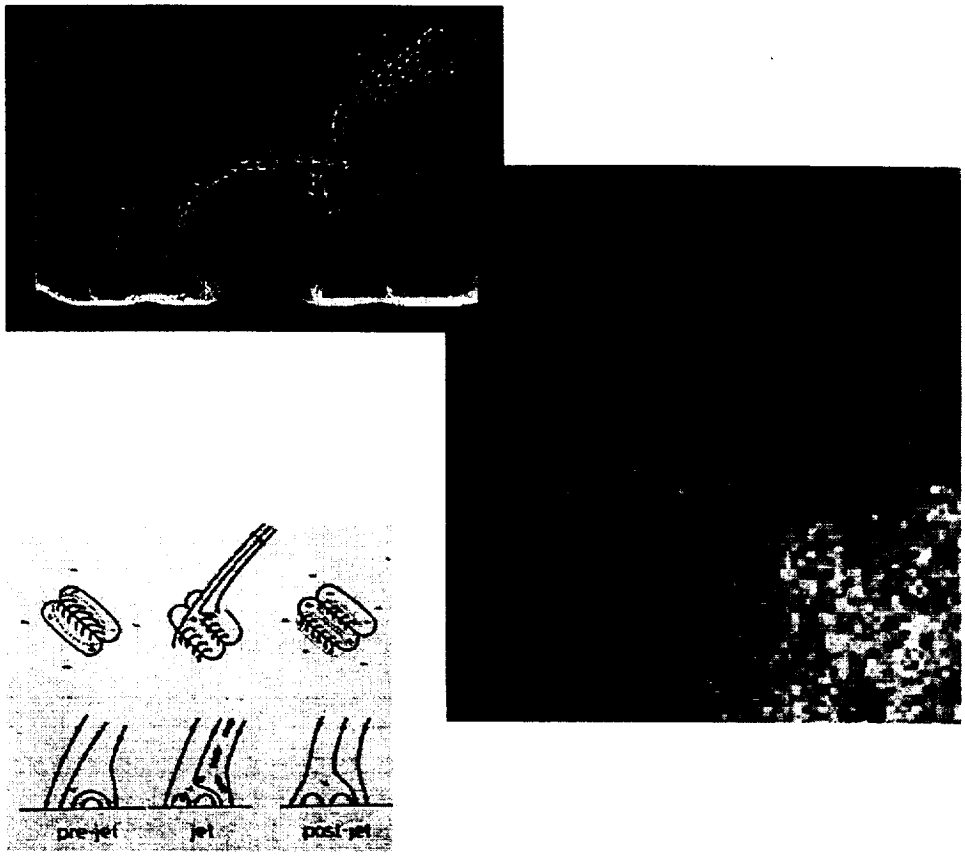

Figure 15: Solar X-ray jet and model. Right: X-ray jet observed by Yohkoh. Left: sketch of magnetic field configuration and reconnection inferred from observations. Top: 2-D MHD simulation.

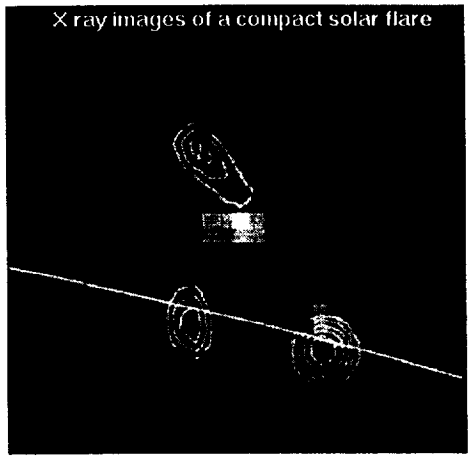

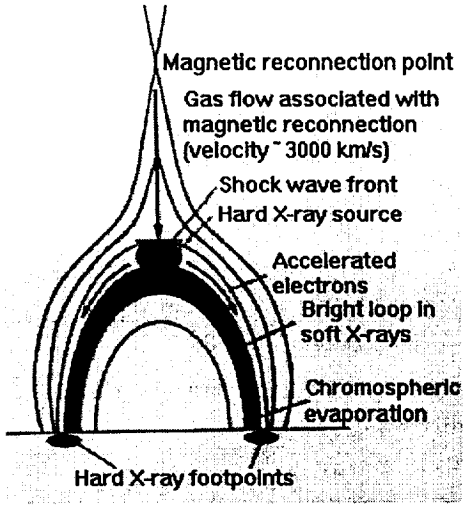

Figure 16: Bright-topped flare images and model. Upper left: compact flare loop observed end-on at limb by Yohkoh: hard X-ray contours superposed on soft X-ray image. Lower right: flare arcade with bright cusp at top observed in soft X-rays by Yohkoh. Lower left: 2-D reconnection picture that Solar-B observations and advanced MHD modeling will test and extend to 3-D.

Theory and Modeling of Solar Eruptions

The study of eruptions that followed the discovery of coronal jets by the Yohkoh team naturally led to attempts to understand the process theoretically, and to model it numerically. The Solar-B data would equivalently revolutionize our view of eruptive events by providing accurate boundary conditions and evolving physical parameters to feed into the models. The 3-D magnetic field data are crucial for producing realistic 3-D simulations of the overall eruptive process. It is only when we can fully simulate the observations in their entirety that we can claim to have answered the above questions.

In the last decade there has been enormous progress in the development of 2-D and 3-D numerical simulation capabilities due to the development of massively-parallel computers coupled with the development of highly sophisticated numerical techniques. The goal of the National High Performance Computing and Communications Program is to develop machines that by the turn of the century will be able to operate at the teraflop rate. With these speeds it will be possible to perform fully time-dependent simulations with grids of order 1024^3, so that we can finally achieve closure between data and theory. Solar-B provides the high resolution observations necessary to test and refine this next generation of numerical models.

3 SOLAR-B INSTRUMENTATION

The over-arching goal of Solar-B is comprehensive understanding of the solar photosphere and corona as a system. Our observational approach addresses this goal through the use of optical and X-Ray/EUV telescopes. We have discussed four specific scientific goals above, and Table 1 links them to specific measurements and instruments. In the strawman payload we describe here, the photospheric measurements are made with a 50 cm aperture visible-light telescope, which is an integral part of the spacecraft structure. This instrument includes both imaging and spectrograph packages in its focal plane. The coronal measurements are made with an X-Ray/EUV imager and an EUV imaging spectrograph.

3.1 Optical Telescope and Magnetographs [1]

We propose to fly a ~50 cm diameter telescope with Solar-B, which would enable us to perform high resolution and continuous observations of magnetic and velocity fields, something we cannot achieve from ground. The focal plane package of the telescope should consist of filter optics and spectrograph. Filters are used for high time resolution observations, in which the narrow-band tunable filter provides 2-D

[1] Abstracted from the Japanese proposal to ISAS

Table 1: Overview of Solar-B Observations and Instrumentation

Science Objectives	Required Observations	Instrument
Magnetic field generation and transport	Vector measurements of the photospheric magnetic field over a large portion of the solar disk for several solar rotations	Vector magnetograph
	The connectivity of magnetic fields through the corona	X-ray telescope
	Location of the sites of magnetic reconnection by means of the Doppler signatures of reconnection jets	XUV spectrograph
Luminosity variation & irradiance	High resolution maps of the Sun's magnetic fields	Vector/filter magnetograph
	High resolution maps of the Sun's radiative output at visible wavelengths	Visible light filtergraph
	High resolution maps of the Sun's radiative output at ultraviolet wavelengths	X-ray telescope, XUV spectrograph
Structure and heating	Measure the transverse motion of small groups of elemental flux tubes in the photosphere	Vector/filter magnetograph
	Determine regions and rates of steady-state and dynamic heating in the corona by measuring densities, temperatures, and velocities	X-ray telescope, XUV spectrograph
	Measure the levels of wave energy in the chromosphere from observed longitudinal and transverse motions	Visible filtergraph, spectrograph
	Search for the existence of sufficient levels of mixed polarity photospheric magnetic fields to test nanoflare models	Vector magnetograph
Eruptive events and flares	Map transverse velocity fields of photospheric flux that produces nonpotential coronal fields	Visible filtergraph, spectrograph
	Measure the magnetic shear at photospheric levels	Visible filtergraph, spectrograph
	Locate the region of intense flare heating	X-ray telescope
	Map explosive ejections of mass from flares	XUV spectrograph
	Detect the initiation and trajectory of coronal mass trajectory of coronal mass ejections	X-ray telescope
	Determine the reaction of pre-existing coronal fields to newly emerging flux	Visible filtergraph, spectrograph X-ray telescope, XUV spectrograph

maps of magnetic and velocity fields and the interference filter provides high-quality images. At the same time, the spectrograph allows us to obtain three components of the photospheric magnetic field with high precision (although on relatively slow time scales).

We anticipate spectacular results coming from this experiment, since it is the first optical telescope from space that allows us to continually observe the Sun in high spatial and spectral resolution unattainable from ground. We can study fundamental problems in solar physics such as identification of fine flux tubes, dynamics of emerging flux, and, in combination with simultaneous observations with the X-ray telescope, mechanisms of coronal heating. In particular, improved spatial resolution leads to detection of smaller current elements, i.e. change in magnetic field energy, which is essential in understanding how the photosphere and corona are coupled. High precision measurements of photospheric vector fields render possible quantitative discussions of many subjects, which we cannot do on the basis of groundbased data.

Background – Limitations of Groundbased Optical Observations

The primary objective of Solar-B is comprehensive understanding of the photosphere and corona as a system, using optical and X-ray/EUV telescopes. Needless to say, we need to design the optical telescope extremely carefully to achieve the primary objective, especially since optical observations can be done from ground. First of all, we set the target spatial resolution to be $\sim 0\farcs2$, in order to detect fine flux tubes. With this in mind, we have evaluated the quality of the best groundbased data and the recent image processings that have been utilized to reduce seeing effects.

La Palma, in the Canary Islands, is widely believed to be the best site to observe the Sun. We have evaluated the data that were taken during a joint observing campaign between the Royal Swedish Observatory at La Palma and Yohkoh (1992 May–July). Some snapshots indeed seem to have resolution better than $1''$, but the average resolution is found to be $1''$–$2''$. We have thus confirmed that the target resolution of $0\farcs2$ cannot be achieved continuously from ground. Moreover, magnetograms and maps of velocity fields require summation of several images, making it difficult to improve the precision because of atmospheric effects (misalignment and image distortion).

Three methods have been used to alleviate seeing effects: (1) adaptive optics, (2) real-time frame selection, and (3) speckle image restoration. Adaptive optics is useful for point sources, but but has not yet been developed for extended and low contrast objects like the Sun. Real-time frame selection technique has been around for a while and is known to be useful, but the resolution it can constantly provide is far below what is required by Solar-B. Speckle image restoration has difficulty making the field of view wide enough, and also quantitative analysis. Another attempt

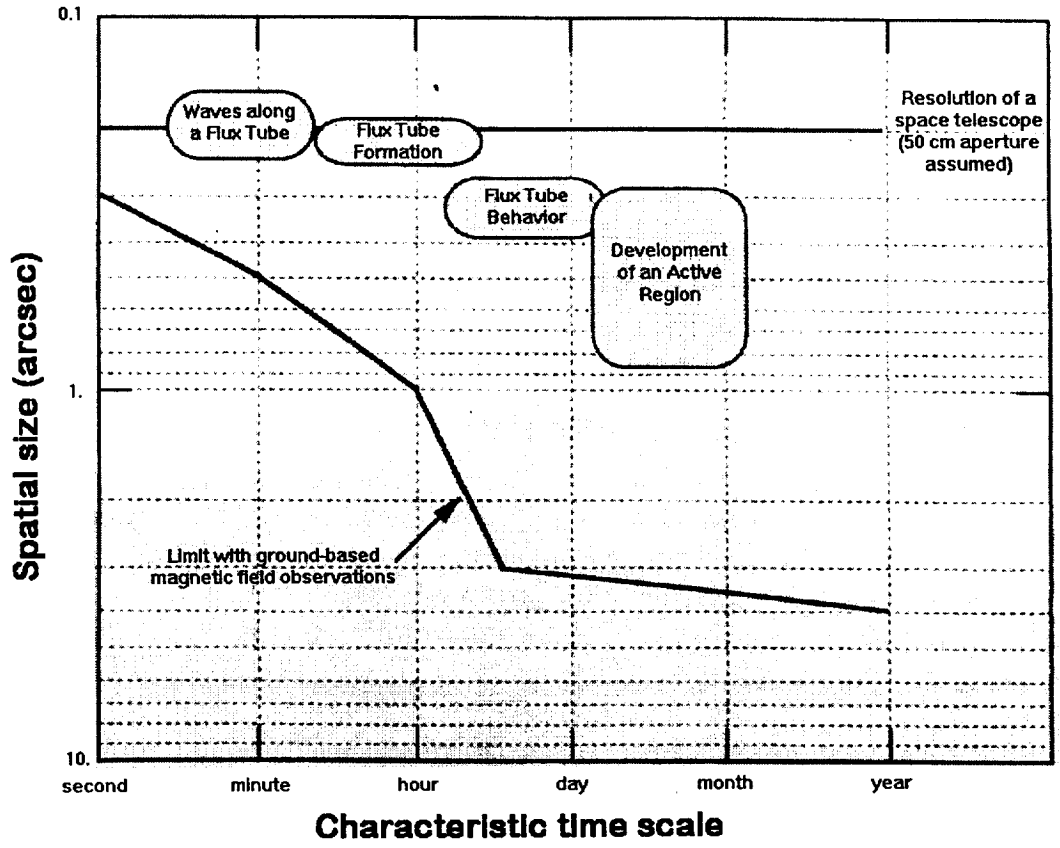

Figure 17: Comparison of space and groundbased observations of solar magnetic fields in terms of spatial resolution attainable and observing time needed. The abscissa is the time period needed to observe the phenomenon. The ordinate is the average spatial resolution that must be obtained within the time of observation, with the highest spatial resolution ($\sim 0''.1$, about 70 km) at the top.

has been to observe infrared lines which are more Zeeman-sensitive, trying to obtain information on the filling factor and structures smaller than the instrumental resolution. Again, this method fails to resolve individual flux tubes and to obtain their temporal developments.

Figure 17 gives a schematic comparison between resolution achieved from ground and from space. Higher spatial resolution imaging alone is an advantage over ground-based observing, especially since we no longer have to worry about atmospheric disturbances. More importantly, high quality magnetic field measurements using stable images are what make observations from space irresistible. Moderately high resolution optical observations from space have been carried out only once for a short period (Spacelab-2 in 1985 with a 30 cm telescope). The proposed telescope for Solar-B will be much better than the predecessors, either on the ground or in space.

Projected Performance of the Optical Telescope/Magnetograph

Here we summarize from the observational standpoint what performance the optical telescope/magnetograph should have.

- Spatial Resolution and Field of View

  The target spatial resolution is $\sim 0\farcs2$, because we want to identify individual flux tubes. This leads to $\sim$50 cm diameter for the primary mirror and $0\farcs1$ pixel size, representing optimal sampling for diffraction limit. The field of view should be at least $200'' \times 200''$ to cover a typical active region expected around the time of the mission. Therefore we will use a 2K$\times$2K CCD as the detector.

- Observing Wavelengths and Spectral Resolution

  With the optical telescope/magnetograph, we try to obtain information on the velocity field and dynamics of fine structures at the photospheric and chromospheric levels and the detailed vector magnetic field in the photosphere. Different wavelengths should be used to cover these different observables. Table 2 lists primary wavelengths and associated spectral lines that are being considered for the telescope. Information on the photospheric magnetic field, which we consider to be of the highest priority, will be obtained by measuring polarization in absorption spectra, which is due to the Zeeman effect. The width of the Fe I 6303 Å line, which is optimally sensitive to magnetic field, is about 100 mÅ and so we could in principle estimate the field strength by measuring polarizations with a comparable spectral resolution. However, the polarization depends on the temperature structure and velocity field of the solar atmosphere, requiring us to observe the line profiles with much better spectral resolution. Our target spectral resolution is $\sim$25 mÅ.

Table 2: Primary Observing Wavelengths

λ (Å)	Ion	Observable	Focal Plane
3933	Ca II (K)	chromospheric heating	interference filter
4305	G-band (CH)	dynamics of granules, structure of faculae	interference filter
5173	Mg I	chromospheric magnetic field (g_{eff}=1.75)	narrow-band filter
5250	Fe I	photospheric magnetic field (g_{eff}=3.0)	narrow-band filter
5576	Fe I	photospheric velocity field (g_{eff}=0)	narrow-band filter
6302/6303	Fe I	photospheric magnetic field (g_{eff}=2.5)	spectrograph
6563	H I (Hα)	chromospheric structure Hα flare	narrow-band filter

- Time Resolution and Continuity of Observations

  The characteristic time scale that controls solar surface phenomena has a wide range of $\lesssim$1 minute to several months. For example, convective cells in granulation change with the time scale of a minute. The yet undetected waves (such as Alfven waves) that are excited in the convection zone and propagate into the corona have estimated periodicities of a few tens of seconds to a few minutes. The time scale of emerging flux is about 30 minutes. Global changes in active regions take place with the time scale of several hours, as seen in X-ray observations. Active region evolution/diffusion has a time scale of a week to several months. Generally, phenomena on small (large) spatial scales have short (long) time scales. Therefore, we envision our time resolution to be about 10 seconds (corresponding to the time needed for sound waves in the photosphere to cross the distance of one pixel) for observations in a small field of view and several minutes to 2 hours for observations that cover a whole active region. The Sun-synchronous orbit ensures continuous observations of an active region while it crosses the disk (up to 2 weeks).

- Precision of Polarization Measurement

  Our ability to measure weaker field and thus to detect smaller changes in energy increases with the precision to measure polarizations in an absorption line. The S/N ratio in the measurement is proportional to square root of the number of photons, so improvement of precision requires long integration times to get more photons. We aim at achieving precision of 0.1–0.2 % per pixel. This allows us

Table 3: Filter Optics and Spectrograph

Item	Filter Optics	Spectrograph Optics
Measured	2D space	1D space×wavelength
Scanned	wavelength	1D space
Data Cube	2D space x polarization x wavelength x time	(1D space x wavelength) x polarization x 1D space x time
Spectral resolution	70–100 mÅ (narrow-band filter), 10–20 Å (interference filter)	25 mÅ
Advantage	Obtain 2D information in a short time	Obtain line profiles with high spectral resolution and accurate determination of the magnetic field
Disadvantage	Hard to attain high spectral resolution or line profiles	Slow to scan

to observe the longitudinal magnetic field down to 2 G. In this way, we will probably be able to detect changes in the magnetic field due to minor flares.

- Two Focal Plane Packages – Filter and Spectrograph –

  As explained above, we are quite ambitious about what we hope to achieve with the optical telescope/magnetograph. It is clearly impossible for one focal plane package to cover all the objectives. Therefore we propose to have two focal plane instruments, filter optics and spectrograph optics, to which we assign complementary roles. The spectral resolution of the filter optics is only $\sim$100 mÅ, not enough for high precision polarization measurements. But the filter optics can simultaneously produce wide field-of-view images and provide high time resolution observations. The spectrograph needs time for scanning different locations to produce a map, but it can provide line profiles with high spectral resolution, which are essential in obtaining accurate vector magnetic field values. Table 3 summarizes characteristics of both the instruments. We expect to achieve our various scientific objectives by using the two packages in accordance with the observing targets. In addition, we plan to introduce table-based flexible observing sequences, in order to achieve the best performance of the telescope for the individual targets.

Table 4: Specifications of the Optical Telescope/Magnetograph

Optical System	Aplanatic Gregorian, 50 cm diameter, F/10.5		
Telescope Tube	CFRP (graphite epoxy), truss structure		
Focal Plane Package	Narrow-band filter	Interference filter	Spectrograph
Objective	Mapping of magnetic and velocity fields	High spatial resolution imaging	High precision magnetic observations
Observing Wavelength	4500–6600 Å	3933, 4305 Å	6203/6303 Å
Wavelength Switch	Rotating waveplate or piezo electric actuator	Filter wheel	—
Spectral Resolution	0.1 Å at 6000 Å	10–20 Å	25 mÅ at 6000 Å
CCD	2048×2048	2048×2048	2048×2048 (TBD)
Pixel Size	$(9\ \mu m)^2$	$(9\ \mu m)^2$	9 μm (TBD)
A/D Converter	10 bit	10 bit	10 bit
Plate Scale	0.″1/pixel	0.″1/pixel	0.″1×25 mÅ/pixel
FOV	$(200'')^2$	$(200'')^2$	150″×0.″2
Standard Exposure	200 msec	0.1–100 msec	300 msec
Time Resolution	10 sec (best)	several sec (best)	100 min/AR
Observing Coverage	Continuous observing in Sun-synchronous orbit		
Image stabilization	Use attitude control and tip tilt mirror to achieve 0.″02 per 10 sec.		
Changing FOV	Spacecraft attitude control (in addition, tracking of a region using solar rotation is under consideration.)		
CPU	Equivalent of 80C386 for control and on-board processing		
Frame Memory	~30 Mbytes (16 Mbit DRAM)		
Amount of uncompressed data	Data production rate: average–740 kbps, maximum–TBD kbps, total amount of data: 4.4 Gbits per orbit		
Number of images obtained	About 440 1k × 1k images per orbit		
Data compression	2×2, 4×4 CCD on-chip pixel summation, bit compression with consideration of photon noise, reduction of the amount of data by using partial-frame mode, DPCM and JPEG compressions by DP		
Size	external: 100 cm × 100 cm × 300 cm		
Weight	goal: 150 kg (maximum system distribution: 200 kg		
Lowest eigen-frequency	15 Hz (assuming that the sub-system requirement is satisfied)		
Moving parts	filer wheel, focus adjustment mechanism, counter wheel (stepping motor) for stabilizing the satellite, shutter (DC motor), tip tilt mirror and scan mirror (piezo electric actuator)		
Temperature control	nominal: Sun light, non-nominal: Night-time heater (TBD)		

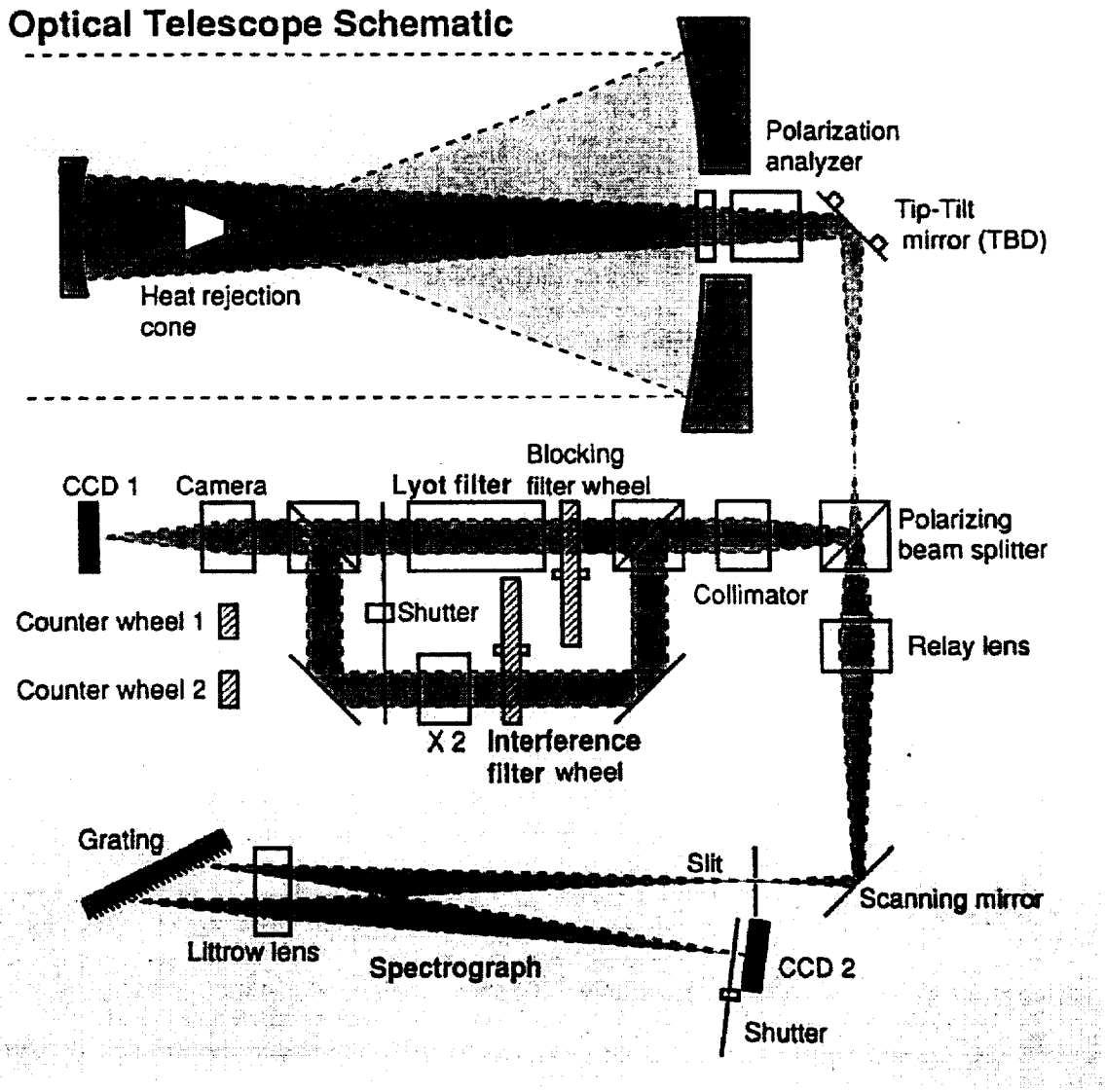

Figure 18: Optical Telescope Schematic. See text for more complete discussion. The polarization modulator, in front of the tip-tilt mirror, is labeled polarization analyzer in this drawing; in fact, the polarizing beam splitter serves as the polarization analyzer.

Table 5: Detailed Parameters of the Telescope Optics

Primary Mirror	55 cm diameter, 50 cm effective aperture, f: 1.5 m, F/3
Material and Weight	ULE or Zero-Dur light mirror (~11 kg) or CFRP+ULE
Surface Accuracy	$\lambda/10$ p-v, $\lambda/40$ rms (including deformation due to gravity)
Support	Multi-point (~9) support from back, 3 interfaces on the telescope structure, stress relief mechanism with springs
Secondary Mirror	17 cm diameter
Synthesized focal length	525 cm, F/10.5 (secondary focus)
Distance between the mirrors	200cm
Back focal length	-24.8 cm
Secondary magnification	3.5
FOV	Maximum $(200'')^2$
Tolerance of positioning the secondary	Along the optical axis: within ± 300 μm, compensated by the focus adjustment mechanism, stability along the optical axis: within $\pm 3\mu$m/TBD interval, inclination: within $\pm 40''$
Heat dump mirror	45 deg flat mirror, aperture: 0.4 cm, external diameter shorter axis D_m: 3.2 cm, shorter axis: 4.5 cm, diameter of the shadow of the secondary mirror D_s: 4.2 cm, margin $(D_s\text{-}D_m)/2$: ± 0.5 cm

3.1.1 Optical Telescope System [1]

We show the layout in Figure 18 and give detailed parameters in Tables 4 and 5. We have established the following baseline for the design:

- The telescope is Gregorian, on the basis of considerations of thermal design. We place a heat dump mirror at the primary focus, excluding sunlight from outside the final field of view.
- The effective aperture is 50 cm, from the requirement of spatial resolution.
- We do not put a tilt mirror in front of the polarization calibration wheel, in order to minimize instrumental polarization and to accomplish the 0.1 % precision.
- To relax the positioning tolerance with the focal plane package, a lens is placed in the center of the primary mirror, collimating the output light.

We include in Table 5 the positioning tolerance for the secondary mirror. We should make sure that the secondary mirror be positioned within ± 0.1 mm (decenter:

[1] Abstracted from the Japanese proposal to ISAS

offset perpendicular from the optical axis) and $\pm 40''$ (tilt: inclination from the optical axis) both in the ground test environment (under 1 G) and in orbit. We plan to absorb this accuracy in the telescope structure design, but if this turns out to be impossible we will put a mechanism to adjust the secondary position. The defocus tolerance of ± 3 μm is worked ont on the assumption of a fixed secondary, and thus should not be regarded as a requirement, as is. Rather it should be regarded as a long-term stability requirement. Therefore it is essential to have a mechanism to adjust the focus, to compensate possible defocus of the secondary mirror and offsets of the components in the focal plane package. With such a mechanism we can cope with the offset of focus caused during launch and secular variations. Apart from vibrations and shocks at launch and initial in-orbit deformation, other causes of focus changes include temperature variations due to seasonal variations of solar radiation input, but this change is slow enough. The positional tolerance of the secondary is set to ± 300 μm, an amount which cannot be compensated by the focus adjustment mechanism in the presence of spherical aberration. As the focus adjustment mechanism, we are thinking of the possibility of moving the collimator lens in the focal plane package or inserting two wedge-like glass plates in the converging optical paths. The accompanying spot diagram in Figure 19 shows the high quality imaging that is expected.

We will choose the mirror material with due consideration in terms of the polishing quality, thermal, mechanical and radiation properties, previous space applications, etc. The present candidates are ULE (ULE7971 of Corning), Zero-Dur and new material that consists of glass with small thermal expansion coefficients placed on CFRP. We plan to adopt either honeycomb or eggcrate structure to reduce the weight of the primary mirror. The weight of the primary mirror is about 11 kg if either ULE or Zero-Dur is used. Thermal deformation is quite small for ULE, as shown in Table 6. So far, the combination of CFRP+low expansion glass is quite unique in the sense that it can satisfy low thermal deformation, high thermal conductivity, light weight and high mechanical strength. We have obtained a 25 cm diameter trial sample and confirmed good surface accuracy in addition to the above properties. The remaining problem is a small amount of warp due to moisture and the way it is supported. Our action items include studying the mechanism to dump heat, deformation and surface accuracy under 1 G gravity, stress relief installation to the telescope body, required centering accuracy, and optimizing mechanical strength and resonant frequency under the M-V vibration environment.

Positioning tolerance of the secondary mirror was obtained through a ray trace with the requirement that everywhere in the $200'' \times 200''$ field of view, aberration (RMS radius) be considerably (less than $1/2\sqrt{3}$) smaller than the Airy disk of a 50 cm aperture primary ($0''.25$ radius at 5000 Å).

[1] AD=radius of Airy Disk ($0.25''$ at 5000 Å)

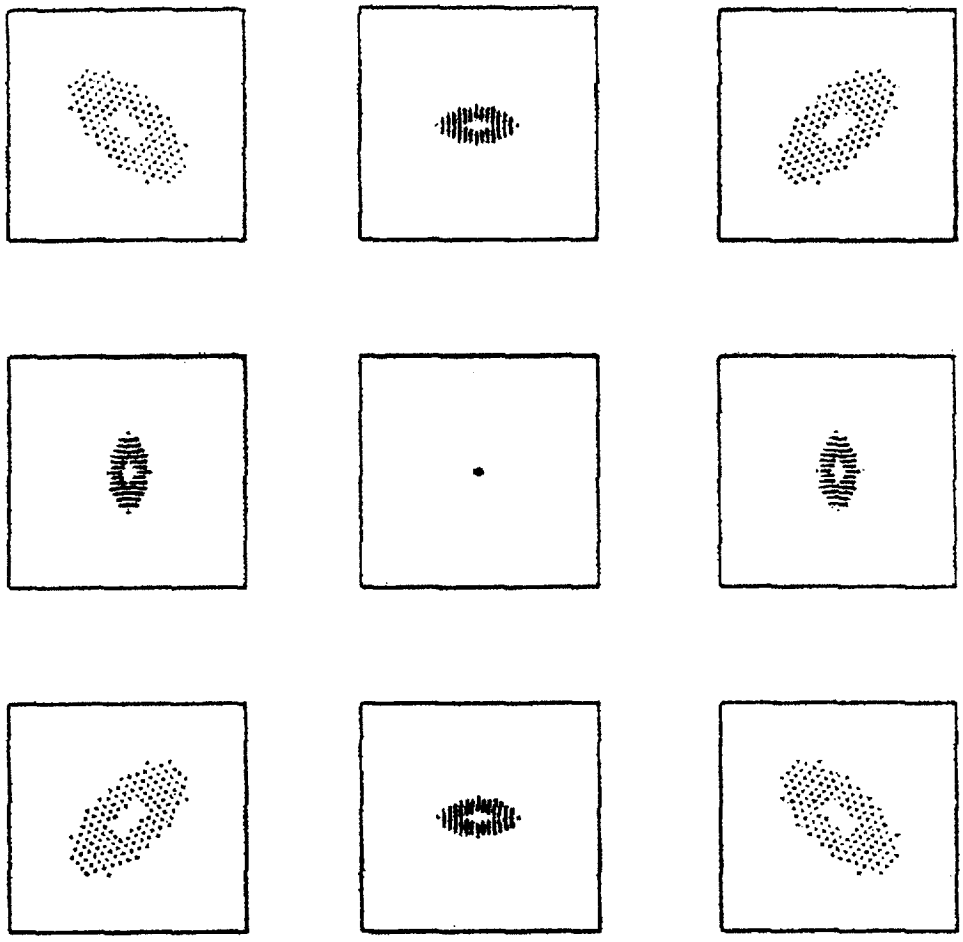

Figure 19: Spot diagrams at the optical axis and 100″ off axis. The 4 corner pixels are located 140″ away from the axis. Each box corresponds to the pixel size (0.″1).

Table 6: Thermal Deformation of the ULE mirror

Pattern of temperature change	type of deformation	effect	
Deviation from the preset temperature ΔT=±50 K	similar	spherical aberration	0.001 AD [1]
Temperature difference between the two sides, simulation using heat input of 32W/50cmϕ	warp	spherical aberration	0.03 AD
Cellular temperature gradient, simulation using heat input of 32W/50cmϕ	scale-like	surface unevenness	$\lambda/10^8$
Radial temperature gradient, dT/dr=-50 K/25cm	bend	spherical aberration	very small

3.1.2 Filter Vector Magnetograph and Imager

General Goals and Specifications

Two filter instruments are discussed here; they will share the optical telescope focal plane with the spectro-polarimeter. For discussion purposes, these systems are referred to as the broad-band filter (BBF), narrow-band filter (NBF), and spectro-polarimeter (SP). The details of how to best integrate and share the resources available behind the telescope focal plane are the subject of ongoing discussions among US and Japanese investigators. However, some goals are clear at the present stage of those discussions.

The BBF should preserve the highest angular resolution of which the telescope is capable while simultaneously covering the entire high-quality field of view (i.e. 200″). The photometric precision and accuracy should be no worse than a few tenths of a per cent in a single exposure. These requirements imply a ccd camera with approximately 0.1″ pixels and a format of about 2048 by 2048 pixels. The spectral ranges to be covered should include the chromosphere (e.g. 393.3 nm), the temperature minimum (e.g. 430.5 nm), and a clean continuum (e.g. 451.9 nm). The spectral resolution should be at least 400. Exposure times should be short enough to reduce any photometric errors arising from the proper motion or evolution of solar features to less than 1%.

The NBF should also meet the same goals as the BBF except for providing higher spectral resolution (at least 50000), a selection of spectrum lines, rapid tunability, and polarization selectability. At least one spectrum line should be chosen to yield high quality photospheric vector magnetic field information. Another spectrum line

should have no Zeeman sensitivity to enable high-quality Doppler shift measurements. Additional spectrum lines that provide magnetic field information higher in the photosphere or in the chromosphere would be highly valuable. A severe challenge is to obtain all the polarization information needed to define the vector magnetic field in a time sufficiently short (seconds) so that line profile variations and solar evolution do not introduce significant errors. Polarimetric accuracy of 0.2% implies inferred magnetic field noise of about 8 and 60 gauss respectively for the longitudinal and transverse field components. These noise levels are targets for single vector magnetograms.

The results expected from the NBF/SP system include: accurate measurements of the azimuth of the traverse component of B in the photosphere and thus more accurate estimates of magnetic topology, accurate calculations of electric currents, magnetic free energy, Lorentz forces and field gradients, accurate measurements of emerging flux and flux cancellation, accurate determination of the photospheric flow field, interplay between horizontal and vertical velocities and location of shear and emerging and canceling magnetic flux, and the role of flows in organizing magnetic field on all scales.

Strawman Filter Instrument

The actual filter system will be selected by NASA and ISAS as the result of an announcement of opportunity. The purpose of this section is to indicate one credible way to obtain high-quality magnetic field measurements with a filter system in the context of limited resources. The strawman described here is based on one prepared as part of the 1996 Japanese proposal to ISAS. Many other concepts consistent with available resources are possible. Note that the focal plane must be shared with the spectrograph.

As indicated schematically in Figure 18, the beam from the telescope passes first through a collimating lens and then through a wheel with various retarders and calibration elements mounted in it. A pupil image is formed on a mirror that can be rapidly tilted to compensate for small spacecraft pointing errors. In this concept, the correction signals are derived from gyro information but it is recognized that additional information from a focal plane image will probably be required. The beam then passes through a lens that collimates the pupil image and then through a rotating retarder and polarizing beamsplitter. These elements serve to select the state of polarization fed into the NBF and BBF systems. The BBF beam passes through a wheel that contains interference filters. It then passes a shutter, a beamsplitter, a camera mirror and is finally focussed on a ccd camera. After the NBF beam leaves the polarizing beamsplitter it passes through an interference prefilter mounted on a wheel and then into a Lyot type filter. Exiting the Lyot filter, the NBF beam passes through a shutter, into the final beamsplitter and then follows the same path as the

BBF to the ccd.

The ccd camera has 2048 by 2048 pixels with each 9 by 9 μm pixel covering 0.″1. A 10 bit A/D converter will provide adequate dynamic range and signal to noise ratio. Exposure times will be 0.1 to 100 msec for the BBF and about 200 msec for the NBF. Each full-frame exposure will produce raw images of 42 Mbits. On-chip binning and partial frame readout will be provided. The data handling system will be able to do simple arithmetic on stored images and both lossless and lossy image compression. These techniques are required since without them only 47 raw images per orbit could be downlinked neglecting the SP entirely.

A representative observation sequence might consist of one BBF frame, one frame each in the red, center, and blue wings of the H-alpha line, and four frames each in the blue and red wings of the magnetograph line (four states of polarization), for a total of 12 frames. Such a sequence would be repeated every few minutes. Note that on-board processing and compression make such a program compatible with the available telemetry.

Heritage

Filter-based imaging and magnetograph systems have a long heritage. Ground-based systems of this sort have been in service for more than 20 years. A current count shows at least ten filter vector magnetograph instruments operating at ground-based observatories. Three additional ones are reported to be under construction and two have been prepared for flights on large, balloon-borne telescopes. A filter magnetograph (longitudinal component only) is on board SOHO and provides excellent measurements. Most of the instruments use Lyot filters but a few use Fabry-Perot narrow band filters. A couple are hybrids that combine Lyot and Michelson filter elements. Polarization modulation is done by variable retarders including KDP and liquid crystal devices, rotating fixed-value retarders, and, in one case a fixed beam-splitter. The polarimetric noise is a few per mil typically. Most of the systems use pass bands of about 0.1 Å and most operate with the 6302 Å line. Other popular lines are 5324 and 5250 Å.

3.1.3 Spectro-Polarimeter

The Importance of Spectrographic Stokes Polarimetry from Space

Quantitative measurements of the photospheric vector magnetic field are fundamentally important to the science goals of Solar-B. Our ability to infer this fundamental property of the solar atmosphere from polarimetric observations depends in a very sensitive manner upon the completeness and precision of the polarimetric observations. It is crucially important to take advantage of the complete information contained in the spectrally resolved profiles of Zeeman-sensitive solar absorption lines

(the "Stokes polarization profiles"). Without such information it is generally not possible to infer the strength and orientation of the magnetic field with high precision and quantitative detail, especially in regions outside of sunspots. Because many of the science goals of Solar-B hinge upon our ability to make quantitative measurements of the field (vertical current densities and true magnetic flux measurements are two obvious examples of required measurements), the baseline concept for the complement of instrumentation aboard Solar-B includes a spectrographic instrument whose primary goal is the precision measurement of polarized solar line profiles. Furthermore, this instrument would perform spatial maps of the solar surface in order to construct detailed, high resolution, quantitative surface maps of the vector magnetic field, maps of related thermodynamic properties of the solar atmosphere, and even point-by-point gradients of these quantities along the line-of-sight from asymmetries of the line profiles.

To date, no instrument capable of vector magnetometry has been flown in space. In fact, it is only within the past few years that the instrumentation with the spectrographic capability described above, along with the analysis methods needed to interpret such data, have been demonstrated through ground-based observations. The recent experience with ground-based spectrograph polarimeters has set a new standard for both precision and angular resolution of vector magnetic fields, and numerous discoveries regarding the nature of the magnetic field, its evolution, and its influence on the solar atmosphere are forthcoming. Figure 20 shows a typical set of polarization images from the ground-based Advanced Stokes Polarimeter. The fundamental data from such a polarimeter are spectral images of the solar photospheric absorption lines in intensity (Stokes I), two orthogonal states of linear polarization (Stokes Q, U), and right- minus left-handed circular polarization (Stokes V), as shown in the lower four panels of this figure. The Q, U profiles are basically symmetric about the centers of the Zeeman-sensitive Fe I lines at 6302 Å, indicating the presence of magnetic fields transverse to the line-of-sight. The Stokes V line profiles are basically antisymmetric. The three images at the top of the figure represent, from left to right, continuum intensity, Stokes V in the wing of one of the lines, and Doppler velocity. They indicate the location of the spectrograph slit corresponding to the spectral images below. The sunspot appears dark at all wavelengths in the Stokes I image. Narrow spectrum lines due to O_2 absorption in the Earth's atmosphere produce no measurable polarization of the spectra. They would be absent in Solar-B spectra. Notable in these spectra is a very small location of supersonic (14 km s^{-1}) downflow visible in the polarization spectra Q, U, V (upper arrow in the Doppler image). Such events would not be recognized in filter magnetograph images. Full spectral polarization profiles of significantly higher angular resolution and polarimetric precision will be obtained by the Solar-B spectro-polarimeter. Data of that quality is necessary to extract precise measures of the vector magnetic field, and other important thermodynamic properties

of the magnetized solar atmosphere. Figure 3 illustrates the spectacular results that we expect to be able to derive on a regular basis from such data.

Stokes polarization measurements are however severely limited by the nature of observing through the turbulent Earth's atmosphere. In order to attain the requisite Signal-to-Noise ratio (S/N > 1000) integration times must be longer than about 3 seconds even with rather large aperture ground-based solar telescopes. With such restrictions, atmospheric seeing sets a fundamental limit – about 1 arcsecond – on the angular resolution achievable with ground based instrumentation, thereby masking much of the information about the small-scale structure of the vector magnetic field. Perhaps more importantly, the 1 arcsecond image quality is quite intermittent, and observational sequences are always compromised by the day/night cycle and by clouds. It is therefore not possible to record the evolutionary history of solar flux elements from the ground with the required precision and angular resolution. For these reasons many crucial observational data on the evolution of the magnetic fields in active regions probably cannot be derived from ground-based measurements.

We are now at a juncture where we understand in detail the the scientific requirements of vector magnetic field measurements, how to carry out the needed precision polarimetric observations from a space platform, and how to interpret the data once it is in hand. It is clear that the entirely new class of observational data afforded by a spectrographic polarimeter in space, operated in concert with the filter vector magnetograph, will represent an unprecedented advance for solar physics in defining the observational state of the solar magnetic field. At this moment we are presented with an extraordinary opportunity: an opportunity which may be seized with relatively modest resources. Such an instrument, along with the suggested complement of other instruments aboard Solar-B, will deliver data which will have a tremendous and lasting impact on the discipline.

Requirements for Precision Stokes Polarimetry

Requirements for precision polarimetry place strong constraints on the mode of data acquisition. Some of the most important issues are listed below.

- Signal-to-Noise Ratio: For analysis of active region fields, a S/N in the range > 1000 appears to be necessary for inference and interpretation of vector fields. For detailed studies of individual flux tubes, or for studies of the quiet internetwork fields, an even larger S/N may be required.

- Simultaneous Polarization Measurements in Two Spectral Lines: It is essential that two spectral lines with similar response to thermodynamic structure, but differing response to the Zeeman effect, be measured simultaneously.

- Rapid Modulation of the Polarization: The S/N requirements also dictate that a full measurement of Stokes polarization profiles takes place in a time interval

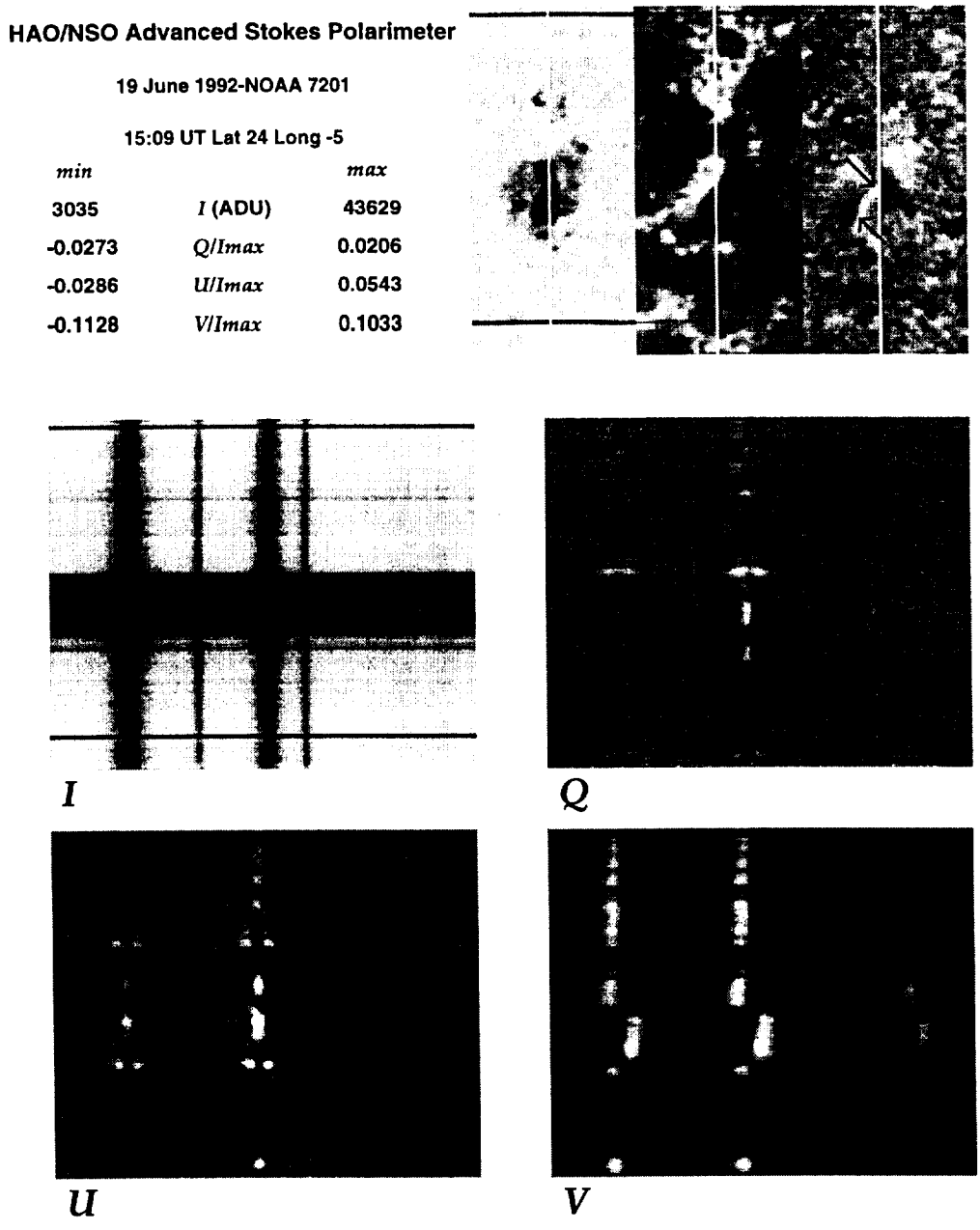

Figure 20: Precision spectro-polarimetric observations of the Zeeman-sensitive Fe I lines at 6301 and 6302 Å.

short enough that there is no appreciable "crosstalk" from intensity into polarization due to evolution of the solar scene. Given expected proper motions of solar photospheric features of a few km/sec, we require that each complete measurement of polarization be executed within less than one second in order to achieve a polarization accuracy of 0.001.

- Efficient Use of Available Light: The strong requirements on S/N dictate that efficient use of the available light flux be made so that maps of active regions may be carried out in a time compatible with their evolutionary time scales.

- Contextual Filter Observations: The spectrographic observations are limited spatially by the width of the slit. Requirements of the S/N and telemetry prevent large, detailed spatial maps of spectro-polarimetric observations to be acquired in a time short compared with the evolution of the solar scene. It is therefore necessary to have BOTH the spectro-polarimeter AND the filter magnetograph operating simultaneously, in concert. In this way, the precision magnetic field measurements from the spectro-polarimeter can be placed into their proper context of the evolution of the solar scene. Such combined measurements are essential to achieve many of the fundamental science goals of Solar-B; for example, in order to both follow the spatial migration of active region flux and to make precise quantitative measurements of the individual field elements.

Elements of the Optical Spectro-Polarimeter

Below we present a strawman concept for the visible light spectrograph, shown schematically in Figure 18. The actual spectro-polarimeter system will be selected by NASA and ISAS as the result of an announcement of opportunity. This concept demonstrates that it is possible to achieve precision measurement of magnetic fields with a modest and simple spectrograph. This concept is only intended as an example to illustrate this feasibility. It is based on studies carried out over the past few years, and a similar system is described in the 1996 Japanese proposal to ISAS. Many other concepts consistent with available resources are possible.

The strawman spectro-polarimeter allows measurement of the full state of polarization in spectral lines formed in the solar photosphere, with sufficient spectral resolution to resolve the subtle features of the Stokes polarization profiles, simultaneously in two nearby spectral lines. It also permits one to acquire measurements of spectra and polarization in the core and wings of the Ca II H-line (3968 A). The H-line measurements are required to connect the photospheric field measurements smoothly through the chromosphere to the upper layers sampled by the other instrumentation on Solar-B. Because of the seeing-free space environment, many of the difficulties associated with ground-based Stokes polarimetry may be relaxed for a space-borne

polarimeter, permitting a smaller, simpler, slower instrument than needed on the ground. Some of the critical elements of this system are described below.

- Polarization Modulator: The polarization modulator is placed as far forward in the optical path as practical in order to minimize the influence of optical elements on the small solar polarization signals to be detected. This device must change the state of polarization of the incident light in a periodic manner. The strawman polarimeter has a continuously rotating fixed retarder with 3/8 wave retardance at the wavelength of the chosen Zeeman-sensitive Fe I line pair at 6302 A. The rotation rate would be approximately 0.94 Hz. An alternate candidate for a polarization modulator is a liquid crystal variable retarder which modulates the retardance via an applied electric field. The former modulation scheme requires a mechanism to rotate the retarder. The latter scheme would require a separate set of polarization calibration optics, in the optical path ahead of the modulator, which could be introduced occasionally to monitor the performance of the liquid crystal.

- Tip-Tilt Image Motion Compensator: Even a tiny translational motion of the solar image at the detector could produce a spurious polarization signal at the limit of the required polarization sensitivity. Gross image translation should be stabilized at the level of about 0.003 arcseconds within the typical time of modulation of the polarization (0.3 seconds). The tip-tilt mirror shown in Figure 18 will compensate for small excursions of the image due to spacecraft drift, vibration from onboard mechanisms, and wobble of the image due to the rotating waveplate. The filter instruments place similar requirements on image stabilization. Note that the solar scene observed at this high resolution will evolve significantly in a few seconds. The tracking cannot compensate for this motion, but polarization errors arising from the evolving solar scene will be smaller than the desired accuracy, 0.001, when the modulation/demodulation of the polarization is carried out at 15 Hz.

- Polarizing Beam Splitter: The image is divided between the spectrograph and the filter instrument via a polarizing beam splitter, which performs several functions. First, it permits simultaneous operation of both systems. Second, it acts as an analyzer for the polarization system, both for the spectrograph and the filtergraph, thus none of the photons available for polarization analysis are wasted in an absorbing polarizer. Third, it acts as the initial polarizer element for the Lyot filter.

- Scanning Mirror: This mirror functions to translate the image of the Sun across the entrance slit of the spectrograph in order to produce spatial maps of the magnetic field and related atmospheric parameters.

- Spectrograph: The simple Littrow configuration, with a total length of about 1.5 m, provides adequate spectral resolution (25 mA) for vector field measurements. The shutter wheel mechanism provides both for dark-level calibration, and contains blocking filters for two wavelengths, 6302 and 3968 A.

- CCD Cameras: The CCD cameras must be read at high rates (15 Hz is the baseline) for the two reasons given above: 1) modulation of the polarization must proceed rapidly in order to minimize the spurious polarization signals from the evolving solar scene, and 2) high S/N requirements demand that photons not be wasted. In the focal plane of the spectrograph the pixels are 0.2 arcseconds by 25 mA. The camera should be a frame-transfer device to permit continuous (un-shuttered) operation, and have low read noise (<60 e-) at the desired 15 Hz read rate in order to achieve measurements dominated by photon sampling statistics. The active area of the chip should be at least 1000 X 200 pixels. Two cameras are required in the focal plane: one for the precision photospheric vector field measurements at 6302 A, and one for the chromospheric spectra of the Ca II H-line at 3968 A. A dichroic beamsplitter preceding these two cameras relay the appropriate wavelength regions to each CCD, and unwanted spectral orders are rejected by broad-band interference filters in front of each camera.

- Demodulation/Accumulation Electronics: The CCD camera is read and accumulated into several buffers simultaneously during about 3 seconds in order to build up the required S/N. A processing system dedicated to the spectropolarimeter will be needed to carry out the demodulation, to cull out the desired spectral and spatial windows from the entire image of each CCD camera, and to apply the lossless or lossy data compression.

Data Rate Considerations

- Maximum Raw Data Rate: 1000 spatial x 80 spectral pixels x 4 Stokes parameters x 2 bytes/pixel every 3 seconds = 2.1 x 10^5 bytes/sec.

- Maximum Raw Data Volume: 1.2 Gbyte/orbit

- Maximum Rate after Data Compression: 120 Mbyte/orbit

- Routine data compression: about 90% is possible without serious degradation of inferred magnetic field parameters.

Table 7: Solar-B Spectro-Polarimeter

Continuum S/N of typical observation	> 1000:1
Polarimetric precision	comparable to noise, i.e. 0.001
Spectral Coverage	Simultaneous coverage of two spectral lines (e.g. Fe I 630.15, 630.25 nm) (Additional coverage of CaII H-line, if possible)
Spatial pixel size	0.2″
Spectral sampling	< 2.5 pm
Spatial coverage along slit	> 200″
Spectral coverage of each photospheric line	> 0.08 nm
Polarization sampling rate (frame rate)	> 15 Hz
Duration for one spectral measurement	< 3 sec.

Critical Design Tradeoffs

- Photon Flux: Calculations based on modern, efficient CCD detectors and other efficient optical elements only becoming available in the last two years, along with the simple optical system of the strawman Solar-B spectro-polarimeter, demonstrate the the strawman system can achieve the required S/N. Additionally, these photon flux estimates have been verified by comparison with actual signal levels from the Advanced Stokes Polarimeter. The projected photon flux remains a serious design consideration of any such precision polarimeter, and any changes of the optical system upstream of the spectro-polarimeter should be weighed in consideration of the stringent S/N requirements.

- Polarization Modulator: Two choices for viable polarization modulators have been considered: a rotating optical retarder and Liquid Crystal Variable Retarders (LCVRs). The rotating optical retarder is robust, but requires a mechanical device and introduces a small, slow, but probably manageable wobble to the beam that must be compensated by an active image motion compensation. LCVRs require no moving parts and do not disturb the beam, but candidate devices are rapidly degraded by UV radiation, and it is not clear how reproducibly their retardance can be tuned, leading to questions regarding the precision of polarimetric measurements possible with such devices. In any case, image motion compensation will be necessary for the optical telescope and instrumentation and it is expected that the high precision needed can be achieved. If the modulator is placed early in the optical path (as is ideally done to allow precision polarimetry), the filter magnetograph, like the

spectro-polarimeter, would need to have a detector capable of demodulating the encoded polarization signal.

- Spatial coverage: The number of CCD pixels along the slit determines one dimension of the spatial maps from such a device. For 1000 pixels, a coverage of 200″ would be possible. This is acceptable for active region studies. Data rate and S/N dictate how rapidly such data can be taken. A reasonable cadence for stepping the slit of 3 seconds (S/N = 1000:1) implies that about 50 min would be required to build up a map of an area (200 x 200″) with 0.″2 steps. Of course, different scientific objectives could dictate larger step sizes, or scans covering a smaller area of the solar surface.

- Data Rate: Any polarimeter such as this will generate a large quantity of data. The instrument outlined in Table 7 will produce a raw data stream with a rate of about 2 M-bit/sec. On-board data compression would be possible to reduce this data flow by a factor of 5-10. Still, this instrument alone could produce data at a continuous rate of at least 200K-bit per second. This is a serious consideration, but this data rate, if not continuous, at minimum would be necessary for extended periods in order to do the science. It should be noted also that considerable on-board processing power will be needed to achieve this level of data compression.

Spectro-Polarimeter Heritage

This instrument has no space heritage, but considerable experience is now in hand from related ground-based instrumentation (the Advanced Stokes Polarimeter: ASP and its predecessors; the University of Hawaii spectro-polarimeter.) The scientific success of ASP and the experience gained with this device has led naturally to a need for more powerful space instrumentation. The need for larger field-of-view than provided by ASP, and the need for observations not limited to a few brief observing runs per year has led to the proposal by the National Solar Observatory for a new ground-based spectro-polarimeter for synoptic studies (as part of the SOLIS facility.) The SOLIS concept has many features in common with the strawman Solar-B spectro-polarimeter presented here. This demonstrates both the scientific need for precision polarimetry and the viability of the overall concept.

It should also be emphasized that a considerable effort has been devoted during the past decade to develop the tools to analyze this data in order to extract vector magnetic field measurements. These techniques are in hand, and are in routine usage. Furthermore, several groups around the world are developing more advanced analysis techniques which now permit the determination of *gradients* of physical parameters, including the magnetic field vector, along the line of sight.

3.2 X-Ray Telescope

The X-ray Telescope is the second major component of Solar-B. It will provide, at a minimum, the detailed observations of the high temperature material in the Sun's outer atmosphere, which in this context includes both the transition region and the corona, in the form of high resolution,full disk images. These images will permit the study of both the dynamics of fine scale coronal phenomena, for instance magnetic reconnection and coronal heating mechanisms, while at the same time recording the large scale global phenomena, such as coronal mass ejections, which have a direct impact on the terrestrial system. A major objective of the X-ray Telescope, which reflects one of the primary objectives of Solar-B, is to observe and quantify the coronal response to changes in the magnetic field measured in the photosphere. This connection has to be made across a relatively large separation in both space (a few seconds of arc) and temperature (1 MK). If the connection for instance between coronal loops and their magnetic footpoints is to be made unambiguously the instrument has to be capable of measuring emission from material lying at least as deep in the atmosphere as the transition region and having a temperature near 0.5 MK. At the same time time the instrument must be capable of recording the emission from the much higher temperature material (2-5 MK) which dominates the corona.

Based on these general objectives a set of minimum requirements for the telescope can be established. First the telescope must have adequate sensitivity over a sufficiently wide wavelength range to ensure that the coronal phenomena can be traced back to the transition region. This specifically implies an ability to detect the emission from relatively cool structures with temperatures between 0.5 and 1.0 MK in the presence, along the line of sight, of material at much higher temperature. Second the instrument must have the ability to provide precise temperature diagnostics over the temperature range from 0.5 to 10 MK. The telescope should be capable of recording the full disk, without raster scanning, and the resulting images should have a resolution defined by the detector pixel size of $1''.25$ (or less), more than a factor of two improvement over the Yohkoh telescope which had approximately $2''.5$ pixels.

In principle the requirements can be met by a telescope based on either the grazing-incidence (soft X-rays) or the normal-incidence multilayer (XUV) mirror approach. Each approach has its strengths and weaknesses and an instrument based on a combination of both techniques deserves serious consideration. This conclusion is based on the evidence, obtained by comparison of nearly simultaneous images from both types of telescope, that they frequently provide a significantly different view of the corona. Such observations may also provide the first opportunity to obtain measurements of the variation of temperature across a coronal loop. Both types of telescope have extensive space heritage. Most recently the extremely successful Soft X-ray Telescope(SXT) on Yohkoh was of the grazing-incidence design while the Extreme

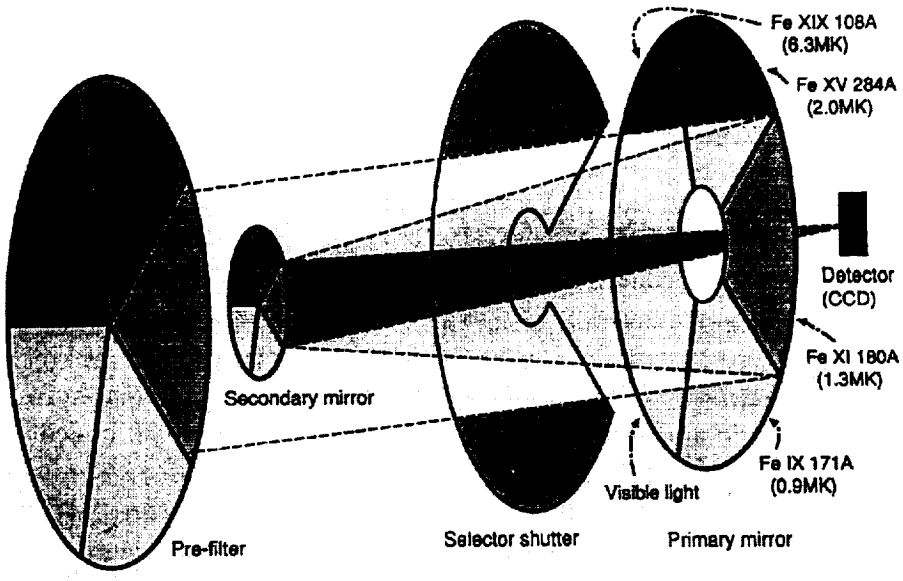

Figure 21: Baseline Solar-B normal-incidence XUV telescope.

Ultraviolet Imaging Telescope (EIT) flown on the SOHO mission and the Transition Region and Coronal Explorer (TRACE) telescope (launch 12/97) employ normal-incidence Cassegrain telescopes, with each quadrant coated with a different multilayer for reflecting a specific wavelength. The lines chosen correspond to low temperatures (below 2.5 MK) and do not cover the full range of interest of Solar-B.

Whichever approach is chosen, grazing or normal-incidence, fabricating the optics to meet the requirement on angular resolution is well within the state of the art. Consequently the limiting factor will be set by the choice of the detector. For Solar-B the use of 2K x 2K CCD detectors in a normal-incidence telescope has been baselined (see Table 8 and Figure 21). Thus for a 1.″25 pixel (a plate scale of 83.″3 per mm) the field of view will be 42.″67 which provides adequate coverage of the corona beyond the solar limb. However it must be realized that the X-ray telescope will be aligned to the optical telescope which will have a relatively small field of view, perhaps 5 ′. If the optical telescope is pointed at a feature near the limb then a significant fraction of the disk will fall outside the field of view of the X-ray telescope, which is an argument for not making the pixels smaller than 1.″25 as this would exacerbate this effect. In a grazing-incidence configuration (Wolter I) the required focal length to provide this resolution is 2475 mm and the aperture of the mirror to provide a suitable collecting area is 300 mm. Thus the envelope for this instrument can be defined as a cylinder with a diameter of approximately 400 mm and a length of 3000 mm. The mass of

Table 8: Baseline Solar-B X-ray Telescope vs. Yohkoh SXT

Item	Solar-B (NI)	Yohkoh SXT (GI)
Optics	Normal Incidence Ritchey-Chretien	Grazing Incidence Wolter I
Aperture Size	20 cm	23 cm
Wavelengths	171 Å, 195 Å, 211+/-2 Å, visible	3-45 Å, visible
Detector	Back-illuminated CCD	Front-illuminated CCD
QE	0.5	0.8
Pixel Size	15 micron	18 micron
	1.″24	2.″46
Format	2048X2048	1024X1024
Field of View	42.′2	42.′0
Geometric Area	45 cm^2	2.62 cm^2
Effective Area	0.3 cm^2 (@171 Å)	0.6 cm^2 (@8 Å)
Temperature Range	0.7-2.0 MK + 14 MK	1.5-50 MK

such a telescope, excluding electronics, should not exceed 25kg. The XUV telescope is assumed to be a Ritchey- Chretien (i.e. an aplanatic Cassegrain) which, with a 200 mm diameter primary and having the same plate scale as the grazing-incidence telescope, could be accommodated within a cylindrical envelope something less than half as long as that required for that telescope, say 1250 mm, and three quarters of the diameter (300 mm) and would have a roughly comparable mass.

The two element configuration of the XUV telescope easily accommodates a factor of four increase in the plate scale in the same envelope as the grazing-incidence telescope, although the field of view is now less than the full Sun and the illumination per pixel has been reduced by the square of the magnification. However the combination of the two telescopes, with the XUV system mounted coaxially within the grazing-incidence telescope, in a single instrument is physically possible and would provide a scientifically exciting opportunity. It would have the capability for making both high resolution observations (0.″5 pixels) of the transition region corona interface where they are most needed and full disk, SXT style images. The availability of both narrow and broad band images would improve the coverage of the temperature diagnostics and would allow the full range of coronal plasma temperatures from < 1 MK to >10 MK to be studied.

The ability to provide good temperature diagnostics will be critical to the quantitative analysis of the Solar-B data. Both telescopes rely on theoretical models of the temperature dependence of the solar spectrum. These are then used to compute ratios of line intensities (normal-incidence telescopes) or selected wavebands(grazing-

Table 9: Goals for an Imaging Spectrometer

spatial resolution	$1''$
spectral/velocity resolution	10 km s^{-1}
temporal resolution	10 s
dynamic range	$> 10^3$

incidence telescopes). Line ratios from the same element are used to avoid abundance differences which makes it difficult to obtain extended temperature coverage. For instance FeIX, FeXI, FeXV and FeXIX provide good diagnostics below 3 MK but are not as good at higher temperatures where the broadband method is quite sensitive. However the broadband method cannot be extended much below 1.8 MK, so that in practice the the two techniques are nearly complementary.

Because of its multiple wavelength bands and the larger CCD the X-ray telescope will be capable of generating over an order of magnitude more data for any specific event than the Solar-A soft X-ray telescope. For instance a 2k x 2k image with 10 bit intensity resolution contains 40 Mbits. Data compression techniques should be able to reduce this by at least a factor of four to a level which is comparable to the Solar-A data rate. However because of the large dynamic range present in X-ray images standard data compression techniques are not as generally effective. Consequently the frequency of full resolution, full disk images will have to be kept fairly low and the telescope will have to be operated predominantly in a windowing or region of interest mode. In this way the demands on the telemetry system can be kept within bounds.

3.3 EUV Imaging Spectrometer

The goal of Solar-B is to understand the solar photosphere and corona as a system. The governing equations of magnetohydrodyamics specify the parameters that determine the state of the solar atmosphere: density, velocity, temperature and the magnetic field as a function of position and time. XUV spectroscopic diagnostics provide strong techniques to determine plasma densities, velocities and temperatures. In addition, it is also possible to determine radiative cooling rates and elemental abundances. A stigmatic spectrometer measures spectral line profiles emitted by the plasmas viewed along the slit. Complete images can be obtained by rastering the slit (SOHO/CDS, HRTS), using a slitless design as in the Skylab spectroheliograph or by a slit/slot combination as in the SERTS spectrograph.

Plasma densities in a narrow temperature range can be determined from line intensity measurements. The intensity of a spectral line is directly proportional to

the emission measure ($\int n_e^2 dl$). With a knowledge of the geometry of the emitting structure the plasma density is derived. This can also be done with imaging instruments. However, the measurement of individual spectral line intensities offers the opportunity to make use of density-sensitive line intensity ratios. The intensity ratio of certain line pairs of several iso-electronic sequence are functions of electron density that can be accurately calculated from atomic parameters. By measuring the intensity ratio of these lines, one can determine the electron density in the source region that is nearly independent of geometrical factors such as the partitioning of the emitting plasma into subresolution structures. A knowledge of the emission measure, the electron density and the geometry of the source can then determine whether or not unresolved fine scale structure are present. These fine scale structures are extremely important for understanding heating through the joule dissipation of electric currents or the viscous dissipation of highly sheared motions, which are expected to occur on small spatial scales.

Only through the understanding of its dynamics can the solar atmosphere be understood. A static atmosphere simply does not represent the important physical processes responsible for the maintenance of a hot outer atmosphere and its often explosive behavior. Clearly, this leads to a requirement to measure the velocities of solar plasmas. The most direct measurement of velocities is through the Doppler shift of spectra lines which can be determined almost solely by spectroscopic techniques. Bulk motions are determined from the net shift of line profiles and the small-scale "turbulent" motions through the width of spectral line profiles.

Spectral lines from any given ion are formed over a narrow range of temperature, typically only a factor of 2. By measuring the intensities of lines formed over a range of temperatures, the variation of emission measure with temperature is found and with this the thermal energy content of the solar plasma as a function of temperature is also known. The plasmas along any line-of-sight to the Sun passes through plasmas at a range of temperatures and spectral line diagnostics provide a good diagnostic for interpreting these emissions. Imaging instruments usually provide only an isothermal or 2-temperature analysis which can over-simplify the analysis of solar phenomena.

By measuring the intensities of several spectral lines spanning a wide range of temperature, the net radiative losses is obtained with the help of a little modeling. The maintenance of the thermal content of the corona against its radiations losses is central to the coronal heating problem.

A good example of the power of spectroscopic analysis are their application to understanding the process of magnetic reconnection. This is a process that is not well understood but always entails the reconfiguration of the magnetic topology of the system and may also result in plasma heating and plasma ejection. It is thought to be a central process in the conversion of energy generated by plasma motions in the photosphere and convection zone to dynamical activity in the corona, such as

coronal heating and prominence eruptions. Spatially resolved spectra can then follow the change in magnetic topology, the increase in plasma temperature, specifying a plasma heating rate, and the velocities and energies associated with the expected reconnection jets. To date, these types of diagnostics have been applied to a few explosive events but Solar-B spectroscopic observations would provide comprehensive information on such key parameters as the rate of plasma heating during reconnection under a variety of dynamical configurations.

Because it is important to observe such small scale transient events as explosive events and microflares, the capabilities of a spectroscopic instrument on Solar-B should be as high as possible. Consequently, the capabilities listed in Table 9 are highly desirable. To measure the flow speeds and nonthermal velocities typical of non-transient conditions, a velocity resolution of about 2 km/s would also be required.

Ideally, the spectroscopic instrument should be capable of observing line profiles of lines formed over a wide range of temperature: 10^4 in the chromosphere, 10^5 in the transition region, 10^6 in the corona and 10^7 K in flares. It is difficult to observe such a complete range with a single instrument operating in a single wavelength region so that it may be necessary to consider the advantages of one wavelength range over another. High quality spectroscopic observations of the Sun have been obtained in the past at X-ray, EUV and VUV wavelengths and can serve as a basis for selecting an appropriate wavelength range.

Instrument

An instrument that addresses the observational requirement for a spectroscopic system is an EUV imaging spectrometer. The EUV spectral region is unique because emission lines of highly ionized elements that are formed over a large temperature range fall relatively near each other in wavelength. Because the lines are near each other, it is possible to design an EUV imaging spectrometer that can observe plasmas formed at temperatures spanning a range from the lower transition region (10^5 K, He II) up to the hottest thermal regions of intense solar flares ($2\text{x}10^7$ K, Fe XXIV). Furthermore, because the lines are close in wavelength, instrumental efficiency differences are small over narrow wavelength ranges, which allows for high relative photometric accuracy. As an example of how close lines can be that are formed at greatly different temperatures, strong lines of Fe XVII ($4\text{x}10^6$ K), Fe XXIV ($2\text{x}10^7$ K), He II (10^5 K) and S XIII ($2.5\text{x}10^6$ K) fall at 254.87 Å, 255.10 Å, 256.32 Å, and 256.69 Å, respectively.

Our strawman instrument consists of a multilayer coated single mirror telescope and a stigmatic (imaging) spectrograph incorporating a concave multilayer coated diffraction grating. Design parameters are shown in Table 10, and a schematic of the optical layout is shown in Figure 22. The instrument operates in the following way.

Table 10: Strawman EUV Imaging Spectrometer Design Parameters

Mirror

Material	ULE
Focal length	150 cm
Diameter	15 cm
Multilayer coating	Mo/Si (Resolution about 10 or less)

Grating

Type	spherical, variable line spacing
Material	ULE
SVLS grating	4800 l/mm
Grating focal length	150 cm
Grating diameter	15 cm
Spatial plate scale	15 microns (2.″1)
	0.0203 A = 15 microns = 20 km/s
Multilayer coating	Mo/Si (Resolution about 10 or less)
Spectral range	240-285 A

Detector

CCD size	2048 x 400
Pixel size	15 microns^2 or less

Pre-filter

Material	aluminum
Diameter	20 cm
Thickness	1700 A
Support	mesh

Primary Focal Plane

Field of view	about 2 solar radii
Solar image radius	about 1.4 cm
Slit	15 microns x (15 x 128) microns
	(2.06 x 264 $''^2$)
Slot	264 x 264 $''^2$
Data Rate	spatial x spectral x no. lines
Spectral mode	256 x 64 x 4
	128 x 64 x 8
Imaging mode	256 x 256 x 1
	256 x 256 x 4
Total data volume	384 mbits/orbit

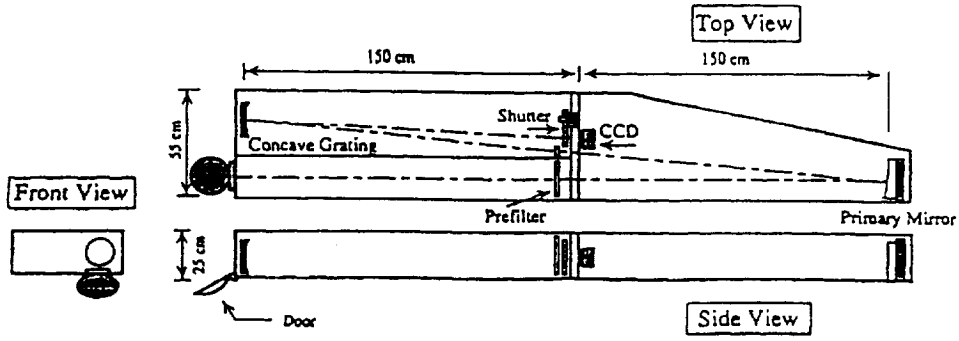

Figure 22: Schematic diagram of the strawman EUV spectrometer.

An off-axis mirror images the Sun onto the entrance slit/slot of the spectrograph. The light is prefiltered by passing the beam through a thin aluminum filter. This rejects the visible light and essentially eliminates concern about scattering in the spectrograph portion of the instrument. The remaining EUV light which passes through the spectrograph aperture is dispersed and re-imaged in the focal plane of the detector. The detector is currently baselined as a 2048 x 400 back-thinned CCD. Other detector concepts, e.g. intensified CCD, may be considered at a later date. The entrance aperture can be either a slit (for Doppler width and shift measurements) or a slot (for spatial imaging). The combination of this aperture configuration allows both imaging and high spectral resolution measurements.

High time resolution and high instrument efficiency can be obtained by using multilayer coatings on mirror and grating surfaces, and by using either a CCD or microchannel plate as a detector. The multilayers are used to enhance the reflectivity of optical surfaces in the EUV region. All optical surfaces are used in normal incidence, rather than grazing incidence. This provides better imaging quality and higher efficiency through large optical surface areas. However, the reflectivity of coatings such as gold and platinum are low in the EUV range, and can be improved by at least an order of magnitude with multilayer coatings.

Our strawman Solar-B EUV imaging spectrometer provides significant technical improvements in several areas over previously flown similar instruments (Table 11).

There are many possible EUV wavelength bands that might be chosen for observation. In the strawman instrument proposed below, the wavelength band is limited by both the properties of the multilayer coatings and by the physical size of the detectors. As an example of a good, but by no means only wavelength region, we have chosen the region between 240 A and 285 A as an illustration. This region is good because it contains strong lines emitted from transition region plasmas through solar flare plasmas. These lines are emitted from He II; Si VII, VIII, IX, X; Fe IX, X, XII,

Table 11: Improvements over Past Instrumentation

Instrument	Improvement
NRL S082-A Skylab spectroheliograph	time resolution and sensitivity (CCD/instead of film) image overlapping is considerably reduced by using multilayer optics
GSFC SERTS rocket spectroheliograph	spatial resolution (longer focal length, superior multilayer telescope, time resolution and sensitivity
ESA/NASA SOHO CDS spectrometer	time resolution and imaging (far superior data rate)

XIII, XIV, XV, XVI, XVII, XXII, XXIII, XXIV; S X, XI, XII, XIII; Mg V, VI, VII; N IV, N V; O IV; and Ar XIII. There are a number of good density diagnostics, e.g., Fe IX, 241 and 244 A. There is considerable temperature discrimination for flares, e.g., Fe XXII, Fe XXIII and Fe XXIV. There is connectivity of coronal plasmas to the transition region through lines of He II, N and O ions, and Mg V. There are both low FIP (e.g., Mg and Si ions), intermediate FIP (S) and high FIP lines (Ar XIII) for abundance measurements.

APPENDICES

A The Solar-B Spacecraft

A.1 Orbit

Solar-B will be launched by an M-5 rocket into a 600-km circular polar Sun-synchronous orbit at 97.79 degrees inclination. Such an orbit has several advantages:

- Continuous solar viewing for approximately eight months, followed by four months with short (up to 20 min) eclipses.
- The long intervals of continuous sunlight greatly simplify the thermal design of the spacecraft.
- Spacecraft motion projected in the solar direction, responsible for Doppler errors in radial velocity measurements, varies slowly (less than ± 0.1 mÅ/s) and over a relatively small amplitude (less than ± 100 mÅ).

The Sun-synchronous orbit includes passages through the auroral zones, as well as the South Atlantic Anomaly. It also exposes the spacecraft to infrequent but intense solar particle events. Table 12 summarizes the properties of the proposed Solar-B orbit in comparison with a standard low-inclination orbit.

To achieve and maintain the proper orbit, the Solar-B spacecraft will require a propulsion system (Hydrazine thrusters).

A.2 Satellite Structure

The principal constraints on spacecraft structural design are

- The optical telescope/magnetograph is bulky and heavy (a package about 1 m diameter, 3.5 m length, and 200 kg mass) and constitutes the central structure of the satellite.
- The optical system has to be well-maintained thermally, considering the solar input, in order to achieve the diffraction limit of 0.2″.

In view of the bulk and precision of the optical telescope/magnetograph instrument (see Table 13), it will dominate the structural and thermal design of the spacecraft. The baseline design concept consists of a cylindrical thrust tube, 1 m diameter x 2.2 m length, thermally controlled by heat pipes, as shown in Figure 24. The thrust tube will also serve as an optical bench for the X-ray and XUV instruments (externally), and will also permit mounting of spacecraft common systems.

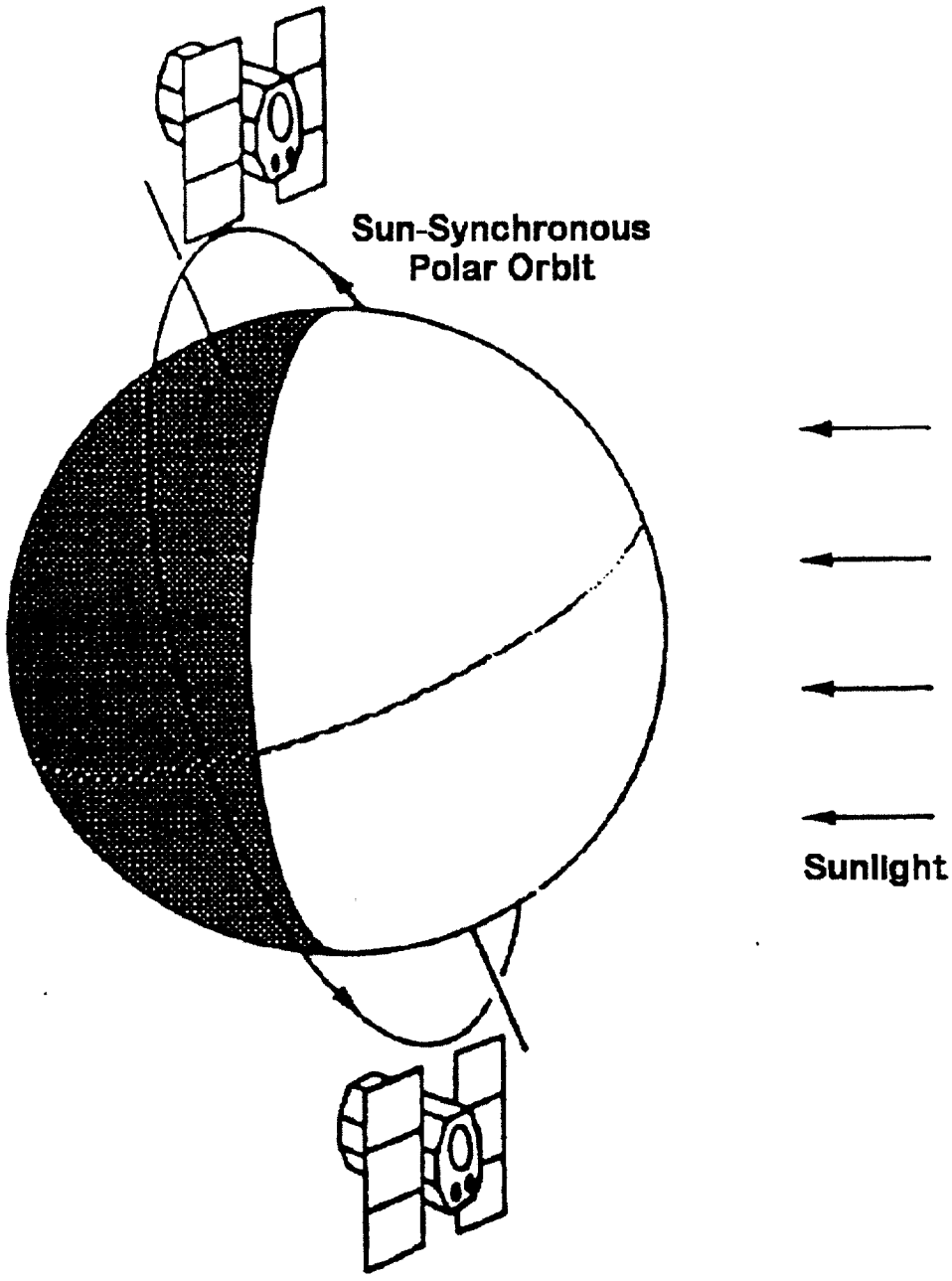

Figure 23: Solar-B's polar Sun-synchronous orbit.

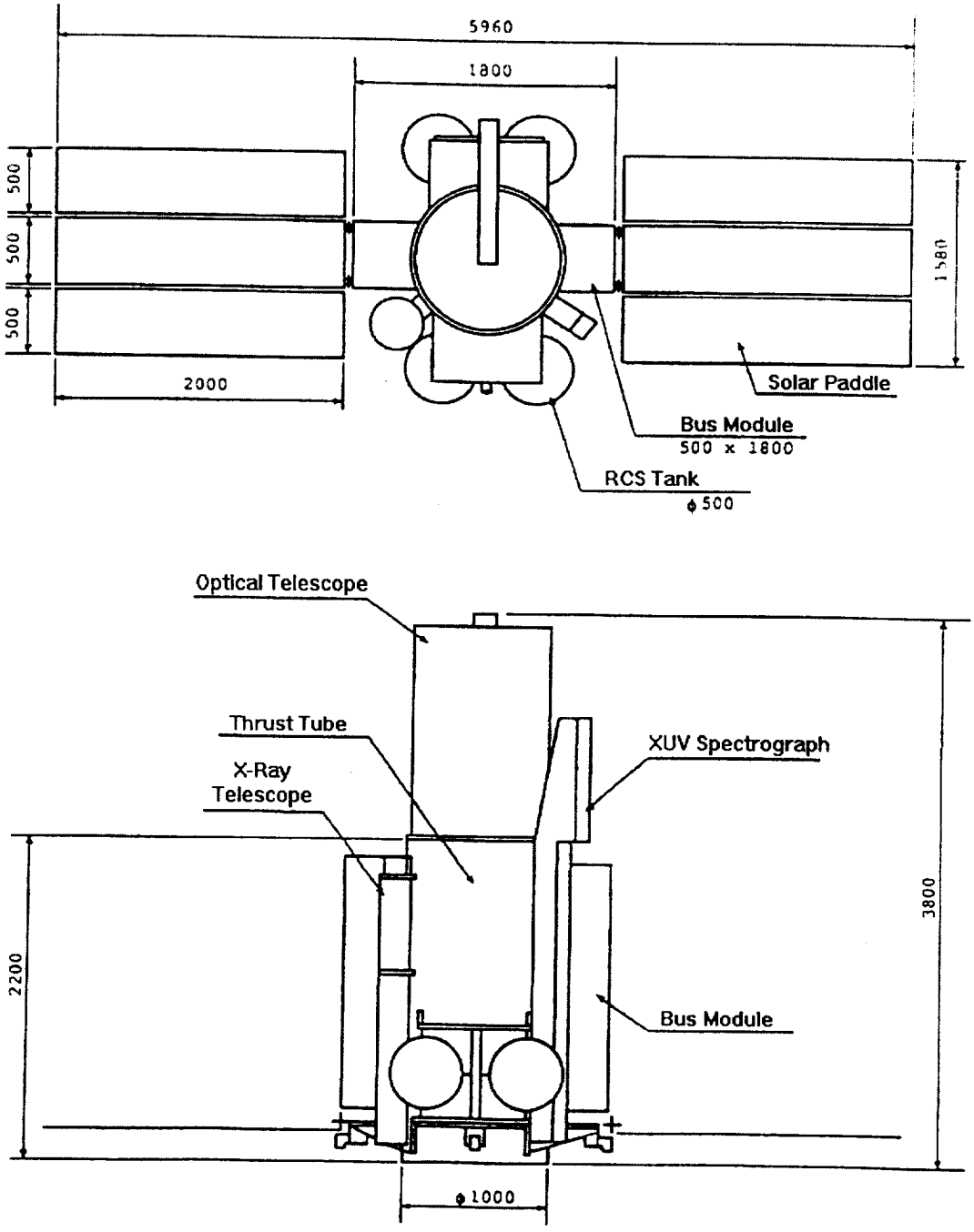

Figure 24: Solar-B spacecraft layout and basic dimensions.

Table 12: Orbit Comparison

Orbit type	Sun-synchronous	Low-inclination
Observations	8 months/year, no eclipse	Eclipse duration 40 minutes per orbit
Doppler shifts	Lower; zero twice a year	250 mÅ p-p (5000 Å)
Power/thermal	Easier	More difficult
Spacecraft mass	850 Kg	1200 Kg
Orbit injection	More difficult	Easier
High-energy Particles	South Atlantic Anomaly Auroral zones Solar particles	South Atlantic Anomaly

A.3 Attitude Control

The Solar-B attitude control systems envisions the use of the spacecraft itself for coarse pointing, plus internal image motion compensation for small angles and high frequencies within the observing instruments as needed. The spacecraft will use a combination of magnetic torquers, gyros, momentum wheels, and possibly momentum adjustment devices to control torques due to internal motions, for example from filter wheels.

Table 14 compares the pointing stability envisioned for Solar-B in comparison with that achieved by Yohkoh. The X and Y axes are orthogonal to the Z-axis, in the Sun-Earth direction; Y is aligned with the solar rotational pole. Table 15 gives the requirements for alignment of the optical telescope, to be achieved by image motion compensation within the instrument itself.

The optical telescope/magnetograph must be able to position its small field of view anywhere on the solar disk, so that simple Sun-center pointing is not sufficient. The field of view may need to track the solar rotation, which is as large as 2 km/s (0.003″/sec) at disk center and is a function (the differential rotation) of solar latitude. To accomplish this a set of on-board reference tables may be used to select a suitable spacecraft pointing motion as a function of observing position on the solar disk.

Table 13: Weight and Power Breakdown

Spacecraft components	Weight (kg)	Power (W)
Dual thruster system	169	
Attitude control system	94	203
Power system	78	5
Telemetry system	11	20
Command/data processor system	13	34
Thermal control system	5	120
Insulation	24	
Support structure	150	
Cable harness	10	
Launch systems	5	
Subtotal	559	382
Payload components		
Optical telescope	200	20
X-ray telescope	30	20
XUV spectrograph	60	20
Particle monitor	6	5
Mission data processor & recorder	10	10
Subtotal	310	75
Total	874	457

Table 14: Pointing precision (peak-to-peak error)

		Solar-B	Yohkoh
Short-term stability	X,Y	$0.2''$/sec	$1.2''$/sec
	Z	$30''$/sec	$5'$/sec
Long-term stability	X,Y	$0.4''$/min	$7''$/min
	Z	$1.5'$/min	$7'$/min
Absolute pointing	X,Y	$< 1'$	$<6'$
	Z	$< 2'$	$<10'$

Table 15: Alignment precision for optical telescope (peak-to-peak error)[1]

10-sec interval	X,Y	0.02″/10 sec
	Z [2]	30″/10 sec
1-minute interval	X,Y	0.4″/min
	Z [2]	1.5′/min
One-hour interval	X,Y	2″/hour
	Z	- [1]

[1] To be achieved by a combination of spacecraft motion and tilt-mirror adjustments within the optical telescope.
[2] Not achievable by measurements within the optical instrument, thus a spacecraft requirement.
[3] See Table 15.

A.4 Data Storage and Transmission

On-board processing

The Solar-B instruments will be capable of generating as much as 8 Gbit per orbit. Even to transmit 10 minutes of observational material would require a downlink rate of 13 Mbps. To handle this problem Solar-B will have hardware implementations of both lossless (DPCM) and lossy (JPEG) compression algorithms. Gate array chips have been developed for this purpose. The Solar-B data system envisions

- Data generation rate, about 500 kbps
- On-board recorder (one orbit's data), about 3 Gb
- Downlink rate, about 5 Mbps

The currently-available HCMOS technology is adequate for the on-board data storage system.

Data transmission

The ISAS programs ASTRO-E and ASTRO-F, which precede Solar-B, will require few-Mbps downlink capability (S-band and X-band at KSC). These systems are close to satisfying the Solar-B requirements. The availability of DSN sites for additional telemetry made many Yohkoh results possible, and the Solar-B program would like also to be able to use DSN. At present, however, the maximum available rate (via convolution coding) is 2.2 Mbps.

B Projected Cost

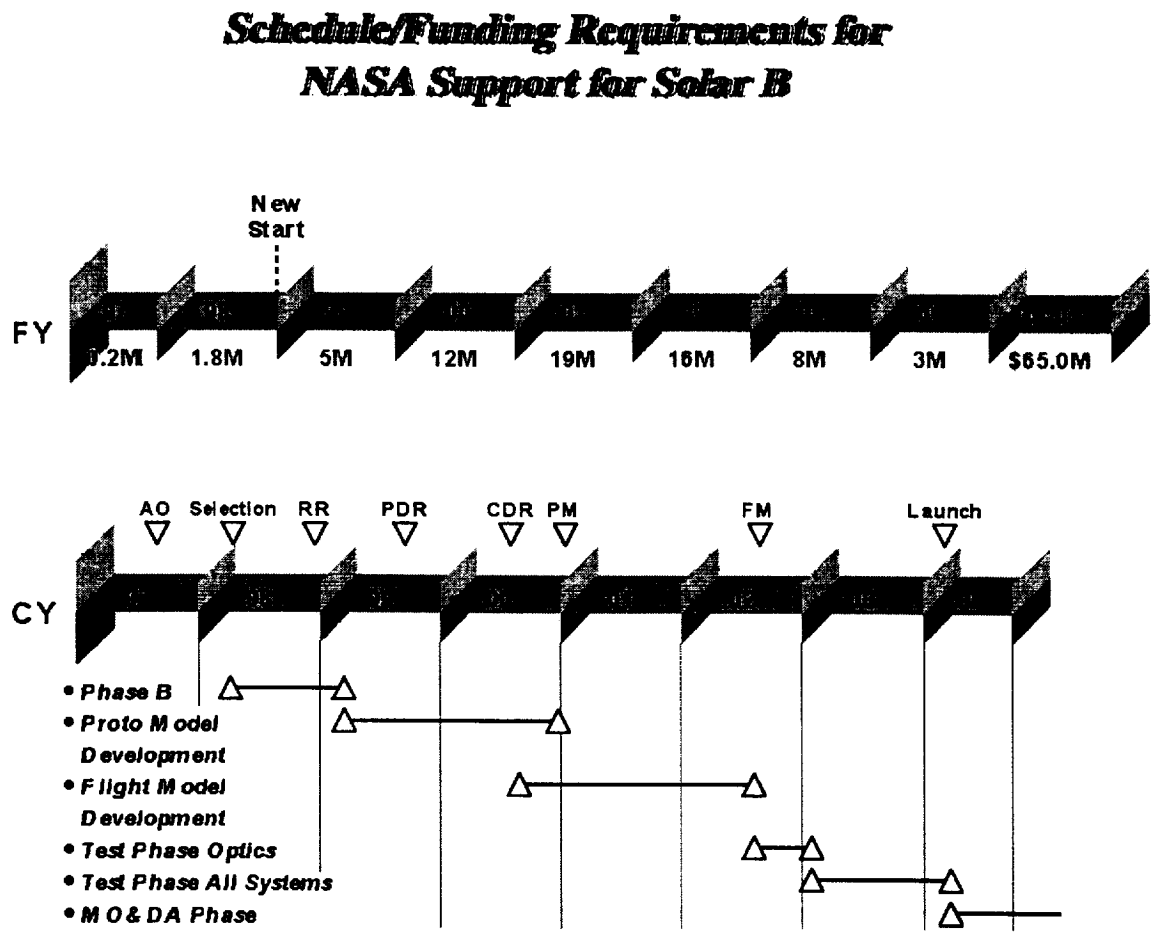

**The total reflects a cost cap established for a launch in 02.*

Figure 25: Projected cost outline for the U. S. contribution to the Solar-B mission, time phased with respect to the major milestones of the ISAS Solar-B program.